

THE PENNSYLVANIA STATE UNIVERSITY
SCHREYER HONORS COLLEGE

SCHOOL OF ELECTRICAL ENGINEERING AND COMPUTER SCIENCE

Developing a Portable Station to Assess Climate Change
and Air Quality in the Central Peruvian Andes

ANTONIO DEMARCHIS
FALL 2022

A thesis
submitted in partial fulfillment
of the requirements
for a baccalaureate degree
in Electrical Engineering
with honors in Electrical Engineering

Reviewed and approved* by the following:

Julio Urbina
Associate Professor of Electrical Engineering
Honors Adviser and Thesis Supervisor

Timothy Kane
Professor of Electrical Engineering
Faculty Reader

* Electronic approvals are on file.

ABSTRACT

This study seeks to develop a portable sensor network tailored specifically to the needs of two agricultural communities in the Central Andes of Peru. The research begins with a broad survey of Peru's climatic state through the lens of global climate change, epitomized by the effects of the El Niño-Southern Oscillation on each of Peru's three areas: coast, jungle, and highlands, the last of which the Junín region partly comprises. Upon more deeply examining the circumstances pervading Junín, the study turns to the residents of Sicaya and Huayao, who offer insight into their climate-related experiences and adaptations (both personal and agricultural) necessitated by increasingly unpredictable climate patterns and meteorological events. Their testimony warrants consideration of Peru's available tools that assess lower atmospheric phenomena: radar-based instruments studying the ionosphere and in situ devices measuring variables directly. However, the still-ambiguous link between upper and lower atmosphere climate change combined with the stationary and sparse nature of existing sensors compels the design and initial testing of a portable, independently powered system measuring three classes of variables: temperature and relative humidity, particulate matter concentrations and size distributions, and greenhouse gas concentrations. The design considers the need for low cost and ease of use in including an independently operating handheld particle counter, a voltage-outputting temperature and humidity probe and gas analyzer, an Arduino Mega controller, and a pair of lithium batteries charged via solar energy. Extenuating circumstances prevent initial testing from fully verifying the system's feasibility in Central Andean operation; nevertheless, the particle counter and gas analyzer demonstrate potential applicational reliability. The study concludes by detailing a future testing regimen that must necessarily precede full system deployment in Sicaya or Huayao.

TABLE OF CONTENTS

LIST OF FIGURES	iii
LIST OF TABLESv
ACKNOWLEDGEMENTS	vi
Chapter 1 What’s the Problem?.....	1
Climate Profile of Peru	2
Profile of Huancayo, Junín, and the Surrounding Area.....	7
Testimony of the Andean People.....	12
Chapter 2 What Tools Currently Exist?	17
Jicamarca Radio Observatory	17
Huancayo Observatory	22
Reviewing Previous Portable Instrumentation Studies.....	34
Chapter 3 Designing a System for Andean Communities	39
Design Principle.....	39
System Components	41
Chapter 4 Conducting Initial Testing	51
Sensor Testing	51
Data Logger and Power Supply Testing.....	63
Chapter 5 Evaluating and Discussing the Test Results	65
Chapter 6 What’s Next?	69
Detailing Potential Future Experiments.....	69
Reflecting and Concluding	73

LIST OF FIGURES

Figure 1: Three climatic regions of Peru (Source: [2])	3
Figure 2: Skyline of Lima, Peru, with flat-top homes visible in foreground	4
Figure 3: Example of terrain outside Lima vulnerable to El Niño-induced landslides	5
Figure 4: Examples of Peruvian Amazon buildings (Source: [9])	6
Figure 5: Average monthly climate data for Cusco, Peru (Source: [10]).....	7
Figure 6: Location of Huancayo within Peru (Source: [11]).....	8
Figure 7: Residential community outside Huancayo, with typical Andean homes visible	9
Figure 8: Aspects of Junín agriculture, as photographed in July 2022.....	10
Figure 9: Example of a field fire (<i>quema</i>) near Huancayo	11
Figure 10: Setting of the Huayao community engagement session on 9 July 2022.....	13
Figure 11: Setting of the Sicaya community engagement session on 15 July 2022.....	15
Figure 12: Main antenna array at the Jicamarca Radio Observatory	18
Figure 13: Gradient Tower at HYO, measuring temperature and relative humidity.....	23
Figure 14: Correlative (top) and temporal (bottom) analyses for temperature and relative humidity during July 2022 (Data obtained from [21]).....	24
Figure 15: HYO black carbon analyzer (left) and external sensor (right).....	25
Figure 16: The Huaytapallana Glacier, as photographed from HYO on 30 June 2022	26
Figure 17: Sun Sky Lunar Multispectral Photometer CE318-T installed at HYO.....	27
Figure 18: HYO weather station (left) along with its data logger, power supply, and solar battery charger	28
Figure 19: Grimm Portable Dust Monitor installed at HYO	29
Figure 20: HYO radar and radiation devices (clockwise from top left): Boundary Layer and Troposphere Radar (BLTR); Ka-band Doppler radar MIRA-35c; radiation instrumentation tower; rainfall estimation radar.....	30
Figure 21: Thermo Scientific 49i and Model 41M ozone analyzers at HYO.....	31
Figure 22: Tropospheric ozone production cycle (Source: [25])	32

Figure 23: Data logging system diagram with Arduino Mega 2560 microcontroller	46
Figure 24: System diagram with LiFePO ₄ battery [41] and DC-to-AC inverter [42] images .	48
Figure 25: SUNER POWER 12 V, 20 W Solar Battery Charger [43]	49
Figure 26: Photographs of larger (left) and smaller (right) Gratury junction boxes	50
Figure 27: Large fire near HYO (photograph taken at 18:59 PET on 19 July 2022)	52
Figure 28: Satellite image of HYO with the four labelled test sites [11, 44]	53
Figure 29: Sample illustration of log file conversion to size distribution plot	54
Figure 30: Setup for test of temperature and humidity probe.....	59
Figure 31: Temperature and humidity plots from the 41382VC probe test in Peru	60
Figure 32: Testing implementation for the LI-850 Gas Analyzer	62
Figure 33: Testing setup for solar battery charger on 22 July at HYO	64
Figure 34: Potential measurement points for Huayao (top) and Sicaya (bottom) [11]	72

LIST OF TABLES

Table 1: Testimony of Huayao residents on several subjects related to climate change.....	14
Table 2: 41382VC Probe image [35] and specifications [36]	43
Table 3: HandiLaz Mini II Particle Counter image [37] and specifications [38].....	44
Table 4: LI-850 Gas Analyzer image [39] and specifications [40]	45
Table 5: Specifications for three battery options.....	47
Table 6: Pre-fire PM measurements at four HYO test sites on 18 July 2022.....	55
Table 7: Post-fire PM measurements at four HYO test sites on 20 July 2022	57
Table 8: Results of preliminary gas analyzer test on 10/18/2022 at 20:40 EDT.....	63
Table 9: Comparative PM2.5 and PM10 measurements for 18 July 2022.....	66
Table 10: Comparative PM2.5 and PM10 measurements for 20 July 2022.....	66

ACKNOWLEDGEMENTS

The author is indebted to Dr. Julio Urbina, whose project coordination and extensive advising allowed this study to occur. Additionally, he thanks Dr. Timothy Kane for his advisory role during the design stage and Dr. Chris Forest, who invaluablely bolstered the project's testing phase. Also, the project relied on the generosity of Dr. Danny Scipión of the Jicamarca Radio Observatory and Dr. José Luis Flores-Rojas of the Huancayo Observatory, who both allowed access to their respective facilities for research.

Additionally, the author thanks the following institutions for financial and logistical assistance: The Pennsylvania State University, the Instituto Geofísico del Perú, the Universidad Nacional de Ingeniería, and the National Science Foundation. This project was supported by National Science Foundation (NSF) Award No. 2107275 to The Pennsylvania State University. Any findings or assessments presented in this work do not necessarily reflect the views of the NSF.

Finally, the author owes tremendous thanks to Gloria Fuentes, Sandra Mendieta, Valeria Llactayo, Jairo Valdivia, David Alejandro, Wilnelia Barea, Jaishree Gupta, and Tarang Shah, among several others, for an unforgettable international experience in a beautiful country with especially kind-hearted people. Also, he appreciates the residents of Sicaya and Huayao for welcoming him to their communities and bestowing him with a new and life-changing world perspective.

Chapter 1

What's the Problem?

Of all conceivable phenomena manifesting themselves as challenges to humanity, one towers above the rest: global climate change. The gradual rise in the Earth's average surface temperature threatens to induce increasingly adverse effects, most notably heat waves and extreme precipitation events. Substantial engineering and scientific efforts seek not only to pinpoint climate change's causes and determine its extent, but also to develop solutions to mitigate the phenomenon before it becomes irreversible. Project Drawdown—which enumerates over 90 such solutions in domains ranging from transportation to agriculture to education—stands as the most prominent mitigation framework following its proposal in 2017 [1]. Indeed, the accelerated warming of the Earth's surface seems to warrant immediate blanket implementation of Drawdown-like solutions wherever feasible, especially considering the global nature of the challenge.

However, despite such a “global nature,” the Earth remains a diverse planet. Each of the six inhabited continents presents a vast heterogeneity of ecosystems, terrains, and human cultures, predicating different situations even within individual nations. Realizing the most efficacious climate change solutions—whether taken from Project Drawdown or not—rests on fully understanding a specific region's social and environmental conditions. Both jointly derive not exclusively from assessing the local atmospheric activity and resultant weather patterns; engaging with residents to comprehensively elicit their experiences forms a critical component, as well. Localizing the climate change issue in this manner—that is, obtaining meteorological data at maximum spatiotemporal resolution and contextualizing it with community testimony—bestows

an engineer with a complete sense of “user needs” through which to selectively design Drawdown-like solutions.

The necessity of such a bilateral approach holds especially true in developing nations. Such countries’ equatorial geographies—combined with their fledgling economic structures—render them especially vulnerable to ever-intensifying extreme weather events. Particularly in more rural agricultural areas, out-of-season frosts devastate crops; heavy rainfall incidents constitute destructive landslides; and extreme temperatures warrant more frequent and interruptive personal adaptations. Understanding these events both quantitatively and through the eyes of the people they affect invaluable contributes to solution development as previously remarked.

Among a plethora of worldwide “natural laboratories” in which to study climate change effects, one nation serves as an effective archetype: Peru. Characterized by a diverse geography—desert and coastline to the west, Andean highlands in the central part, and the Amazon jungle to the east—Peru contains no shortage of communities that hold direct interests in understanding the effects of, and possible mitigation strategies to combat, global climate change. Achieving these ends requires first profiling the country with respect to existing climate information and a more tangible facet: extreme weather events experienced by the Peruvian people.

Climate Profile of Peru

Located on the Pacific coast of South America between the 0.04°S and 18.35°S latitudes, Peru experiences far from the climatic homogeneity expected in tropical-residing nations. As alluded to above, the presence of the Andes Mountains—the longest continuous range in the

world—and the Amazon rainforest longitudinally divides the country into three rather distinct regions: coast (*la costa*), highlands (*la sierra*), and jungle (*la selva*), as illustrated in Figure 1.



Figure 1: Three climatic regions of Peru (Source: [2])

Coastal Region: The westernmost coastal region, which houses the capital city of Lima, maintains a year-round arid, moderate climate under normal conditions. Unlike other tropical areas, the Peruvian coast experiences average monthly temperatures rarely exceeding 25°C, with low temperatures approaching 15°C in September, the coldest month [3]. The Humboldt current—the regular transfer of cold South Pacific water near Antarctica to the tropical latitudes of the Peruvian coast—primarily accounts for such unusually low temperatures [4]. Moreover, the nearby Andes block west-flowing, moisture-rich trade winds [5], preventing substantial precipitation and yielding desert-like conditions throughout the region. The negligible amount of rainfall explains the flat roofs and open building structures along the coast [6]—most prominently in Lima, which comprises Figure 2.



Figure 2: Skyline of Lima, Peru, with flat-top homes visible in foreground

Importantly, the relative climatic stability of the coastal region ceases when affected by the El Niño-Southern Oscillation (ENSO) phenomenon. Every two to seven years, the upwelling of cold Pacific water—which yields the mild conditions highlighted above—reverses, resulting in irregularly warm water off the Peruvian coast. This produces extensive rainfall in the region, sometimes manifesting as extreme events [4], especially during the austral summer months (December to February). The El Niño events of 1982-1983, 1997-1998, and 2016-2017 stand out as particularly destructive, with the most recent yielding widespread flooding and landslides (*los huaycos*) that killed 100 people nationwide [7]. Despite the hemispheric scale of the ENSO phenomenon, Peru's adjacency to the South Pacific renders the country especially vulnerable to the resultant extreme events. Moreover, as the microcosm of the 2016-2017 event illustrates, El Niño episodes have generally increased in intensity; debate persists within the climatology community regarding the role of global climate change in this observed trend. The photograph of Figure 3, taken near the Jicamarca Radio Observatory outside Lima, exemplifies coastal region

terrain that remains susceptible to—and, in fact, shows remnants of—the aforementioned *huayco* events.



Figure 3: Example of terrain outside Lima vulnerable to El Niño-induced landslides

Jungle Region: The Amazon rainforest geographically dominates Peru's east side, accounting for around 60 percent of the country's total land mass. Even adjacent to the Andes, the highest part of the jungle remains around 1000 m above sea level (ASL), portending a similar state of month-to-month climate uniformity, albeit to the opposite effect. Average temperatures in excess of 30°C regularly characterize the region, and annual precipitation totals range from 1000 mm to 3000 mm [8]. Such large amounts warrant vastly different building architectures [6]; Figure 4 pictures typical Amazonian homes with their distinguishing sloped roofs and pillar-raised surfaces.



Figure 4: Examples of Peruvian Amazon buildings (Source: [9])

Highlands Region: The Andes region of Peru stands out as the most climatically dynamic of the three. The high altitudes—extending upwards of 6100 m ASL—combined with the aforementioned nature of the southeasterly trade winds result in erratic changes in average temperature and precipitation quantity throughout the year. Data for city of Cusco in the southeastern Andean subregion serves as an effective paragon of these month-to-month shifts.

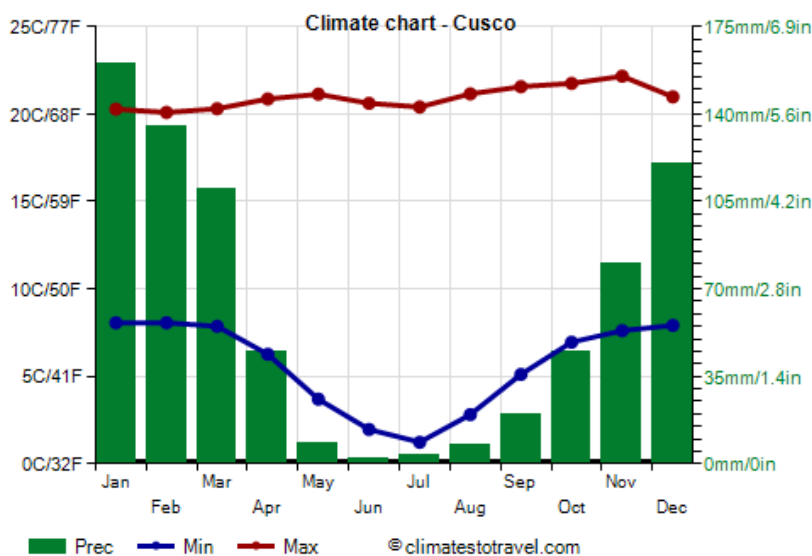


Figure 5: Average monthly climate data for Cusco, Peru (Source: [10])

As evidenced by Figure 5, Cusco—and by extension, the entire highlands region—experiences distinctive wet and dry seasons (constituting the colloquial summer and winter, respectively). Although the Andes seem to climatically isolate the highlands region from the coast, the effects of El Niño extend inland; in fact, “the accumulated rainfall in January [2017]” measured as a 45-year high for four central Andes political regions [10]. One of these, the Junín region, warrants an in-depth examination of its social and environmental characteristics to better understand the localized effects of global climate change. Such an examination comprises the main precursory objective of this study.

Profile of Huancayo, Junín, and the Surrounding Area

Huancayo, the capital of the Junín region of Peru, sits approximately 200 km east of Lima and at 3250 m ASL. The city’s geography, pinpointed in Figure 6 below, affords the previously

mentioned binary seasonal pattern to Huancayo—and to neighboring communities, among which include Chupaca, Sicaya, and Huayao.



Figure 6: Location of Huancayo within Peru (Source: [11])

The typical homes and buildings throughout the region—composed mainly of adobe and consisting of slightly sloped roofs, unlike those in Lima—reflect the people’s adaptations to the climate patterns experienced in Junín [6]. Figure 7 photographs a cluster of such homes a few kilometers outside of Huancayo.



Figure 7: Residential community outside Huancayo, with typical Andean homes visible

Economic activity in the Junín region revolves extensively around agriculture. Crops such as potatoes (*las papas*, several species of nearly 4000 native to Peru), corn (*el choclo*), and lima beans comprise an invaluable part of the harvest, which historically occurs in the month of April. Additionally, livestock farmers raise cattle (*el ganado*), sheep (*la oveja*), llamas, guinea pigs (*los cuyes*), and other animals to sustain the region. Figure 8 illustrates facets of the Junín agricultural situation in July 2022; three months removed from the harvest and in the heart of the austral winter, the time calls for preparing empty fields in advance of the imminent growing season.



Figure 8: Aspects of Junín agriculture, as photographed in July 2022

Occasionally, the fields surrounding Huancayo and the nearby communities catch fire—almost inexplicably from a faraway bystander’s perspective. Even in the agriculturally dormant month of July, such fires (colloquially referred to as *quemadas*) often grow to consume entire subsections of fields, as Figure 9 visually exemplifies.



Figure 9: Example of a field fire (*quema*) near Huancayo

The harmful effects of such fires—both on the land integrity and the air quality—warrant scientific investigation into their causes; indeed, this constitutes the past research of several climatologists. Zubieta et al. attempt to correlate fire incidence in all three Peruvian Andes subregions (southern, central, and northern) with various climatic parameters including cumulative precipitation and frequency of dry days [12]. The authors consult a published dataset for temperature and precipitation figures during the 2002-2016 period. They supplement this data with quantities related to vegetation—e.g., water content as estimated by the Global Vegetation Moisture Index (GVMI)—to directly link fire occurrences to ground and atmosphere conditions. Presenting the results in the form of three parameter correlation matrices, Zubieta et al. demonstrate a possible connection between climate parameters—particularly cumulative precipitation (CP), dry-day frequency (DDF), and hot-day frequency (HDF)—and fire incidence for all three geographic areas except the northern region. Despite the whisker plots incorporating fire events from all twelve months of the year, the domain associated with the climate variables—

and, by extension, the final correlation analysis—stays confined to the May-November timeframe, viz., the typically drier half of the year. The results of the study motivate further investigation of fire causes and effects; perhaps this warrants improving the resolution to a finer scale than the three regions considered in this research.

The efficacy of the Zubieta et al. study aside, research into Andean fires—particularly the *quemadas* directly experienced by local residents—remains empirically limited. The first step toward closing such gaps, and toward posing and answering relevant scientific questions, comprises direct engagement with the Junín residents. Eliciting the people’s experiences with meteorological events and patterns—and their adaptations to them, both with respect to agriculture and their personal lives—remains necessary to more fully understand global climate change’s localized effects—and thus to more finely assess them.

Testimony of the Andean People

Huayao: On 9 July 2022, the residents of Huayao, located approximately three kilometers southwest of the Huancayo Observatory, offered insight into their daily lives through several group engagement sessions. The discussions proceeded an informative lecture on global climate change delivered by Dr. Chris Forest, Professor of Meteorology at Penn State, and translated by Dr. Julio Urbina [13]. Although this seminar constituted the first conceptual exposure to climate change for many attendees, the elicited testimony—particularly the accounts of necessary adaptations to unexpected climatic variations—highlights the community’s indubitable awareness of climate change’s effects. Extracting the people’s most pervading concerns and their most pressing needs

from such discussions allows one to isolate specific, targeted research questions and thus to design a viable and effective means of answering them.



Figure 10: Setting of the Huayao community engagement session on 9 July 2022

Of the approximately 50 Huayao residents that attended the seminar, 10 of them provided specific testimony that Table 1 enumerates [14]. In accordance with Institutional Review Board (IRB) regulations and to preserve the residents' identities, all participants offering insight remain anonymous.

Table 1: Testimony of Huayao residents on several subjects related to climate change

SUBJECT	COMMUNITY TESTIMONY (translated and paraphrased)
Precipitation	Typically, September to March constitutes the rainy, or “wet,” season; however, it shifted a few months late in 2021-22.
Temperature	Throughout 2022, Huayao had experienced drastic changes in intra-day temperatures (specifically in June).
Seasonal Changes	Many in the community had been erroneously informed that the Earth’s receding from the Sun, not atmospheric changes, explains lower dry season temperatures.
Humidity	One resident had recently measured a low temperature of -5°C yet notes that she still felt colder than during another measured incidence of -18°C.
Agriculture	Local farmers had been told to prevent devastating frost onsets by intentionally starting controlled field fires (<i>quemadas</i>), even during the dry season.
Waste Disposal	Several residents had been unaware that burning trash (e.g., tires and plastic) and biomass harmfully impacts the atmosphere.
Home Adaptations	The residents highlighted the annually worsening nighttime cold and want to learn how to heat their homes. Most adobe homes in Huayao lack insulation layers, and according to direct inquiry, none of the 10 residents possess home heating systems.

The surveyed residents asked additional questions regarding climate change—both its manifestations and ramifications. Nevertheless, these stand as auxiliary with respect to the tabulated first-hand accounts of the community’s observations, misconceptions, and adaptations relating to atmosphere-induced phenomena. This warrants further insight from those residing in a neighboring community, Sicaya.

Sicaya: A second climate-related seminar and discussion session occurred in Sicaya, located approximately three kilometers north of the Huancayo Observatory, on 15 July 2022. Both

students and adult residents of the agriculture-focused community learned about global climate change before contextualizing the presentation's content with their personal testimony.



Figure 11: Setting of the Sicaya community engagement session on 15 July 2022

A group of 10 residents—primarily comprised of students—offered testimony revolving around a specific facet of agriculture: frost [15]. One student noted that a single frost event carries the potential to destroy up to half of the crops planted at a given time. Moreover, local farmers realized at one point that flat lands remain more susceptible to frost than slopes; as such, they had transferred many crops to inclined fields in order to avoid frost.

Like the people in nearby Huayao, the surveyed Sicaya residents emphasized the regular practice of starting field fires to prevent frost incidence. Another parallel observation related to the growing irregularity—and thus unpredictability—of the seasonal rain cycles; as a result, both

Sicaya and Huayao farmers increasingly struggle to predict the ideal planting seasons. Because such a great extent of both communities' economies and livelihoods depends on agricultural output, all participants between the two engagement sessions expressed particular concern about the ever-growing difficulty in accordingly modifying farming practices.

The insight provided by the Sicaya and Huayao people demonstrates that the existing static climate profile of Peru fails to adequately characterize the country's experiential situation, especially the Central Andean region. Indeed, learning of the agricultural communities' dynamic adaptations—necessitated by unpredictable atmospheric conditions—compels one to consider how to develop more accurate profiles of such conditions. This, in turn, allows the Andean farming communities to better refine their own practices. A viable starting point for such consideration manifests itself as a rather well-established toolset: Peru's existing atmospheric instrumentation.

Chapter 2

What Tools Currently Exist?

Despite its relatively less mature socioeconomic status, Peru maintains several observatories dedicated to advancing understanding of the atmosphere and, by extension, the climate. Most manifest themselves as facilities owned and operated by the Instituto Geofísico del Perú (IGP). The most prominent of these include the Jicamarca Radio Observatory and the Huancayo Observatory, both of which warrant examination of their instrumentational capabilities and shortcomings.

Jicamarca Radio Observatory

Located approximately 25 km northeast of downtown Lima, the Jicamarca Radio Observatory (JRO) stands as one of the world's main upper atmosphere research sites. Employing 18432 dipole antennas divided into four quadrants, JRO conducts various experiments surveying the ionosphere—the region of the atmosphere between 50 km and 1000 km above the Earth's surface containing high free electron and ion concentrations. As JRO resides almost exactly on the Earth's magnetic equator, any signals propagated directly upward interact perpendicularly with the planet's magnetic field lines, affording nearly ideal measurement conditions. Figure 12 photographs the main antenna array of JRO.



Figure 12: Main antenna array at the Jicamarca Radio Observatory

The facility's engineers and researchers utilize its 49.9 MHz very high frequency (VHF) radar, its 4.5 MW transmission power, its nearly 83000 m² collecting area, and its geographically advantageous location to quantify several upper atmospheric parameters. Most of the obtained data relies on the incoherent scattering radar technique, contingent upon the identically named physics phenomenon involving free electrons and ions. When the JRO-generated 49.9 MHz beam interacts with plasma-bound electrons and ions, the random motion of the particles causes each one to reflect an individual wave, sometimes back to the surface. The nonzero velocity of each charged particle Doppler-shifts—i.e., alters the frequency of—the corresponding reflected wave with respect to the common incident beam. Observing the distribution of reflected wave frequencies at JRO enables one to elicit several physical datapoints characterizing the ionosphere.

For example, Fejer et al. apply the incoherent scattering technique in conjunction with the more sophisticated “oblique mode” to measure evening-hour ionospheric electron temperature increases [16]. Such a method entails operating each diagonally adjacent array quadrant pair

(north-south and east-west) separately; coordinating the two quasi-independent experiments enables accurate results, according to the authors, for altitudes not exceeding 500 km. Fejer et al. seek to extract data from two separate solar events—one occurring in August 2011 and the other occurring in January 2020—distinguished by plasma density reduction. Although the second event produces observed electron temperatures exhibiting high degrees of uncertainty, the measurements from 5 and 6 August 2011 convey a 200 K average electron temperature increase, and a logarithmically proportional electron density decrease, at altitudes in the 250-350 km range around 18:00 local time (LT). The authors succeed in roughly reproducing these empirical results through a simulation that accounts for plasma drift to yield an altitude-temperature graphical relation for both electrons and ions.

Likewise, several researchers highlight the relationship between electron density and certain ionospheric phenomena, as Pedatella et al. do with respect to colloquially defined “150-km echoes”—inexplicable radar echoes that seem to haphazardly occur around the said altitude [17]. The empirical component of their study involves JRO observations made utilizing the Mesosphere, Stratosphere, and Troposphere (MST)-Incoherent Scatter Radar (ISR) technique; this extends the aforementioned incoherent scattering application to the study of the three lowest atmosphere layers, ranging from the surface to 200 km altitude. The authors extract JRO data from the 7 September 2005 solar flare event to hypothesize and to determine the effects of “photoelectrons” on the naturally occurring radar echoes; indeed, this fails to comprise nominal conditions—i.e., no coincident flare activity. To synthesize the JRO measurements, Pedatella et al. run parallel simulations incorporating the Whole Atmosphere Community Climate Model (WACCM), which iteratively profiles the entire atmosphere by linking quasi-independent processes among the several layers. Analyzing the observed radar echo layering structures and carrying out WACCM

Version 4 simulations of electron density, the authors discover relatively consistent quantitative behavior in the moments preceding and proceeding solar flares. However, they conclude that the study's specificity warrants additional testing to better understand the nature of the "still unexplained" radar echoes; moreover, the simulation data weakly correlates with the experimental results for the geographical region containing JRO.

Application of the WACCM, as conducted by Pedatella et al., highlights a critical outstanding research question: understanding the relationship between the upper atmosphere and the lower atmosphere. Global climate change indubitably manifests itself as seasonal pattern changes and increasingly frequent and intense extreme weather events, all of which arise from lower atmospheric processes. Considering the nature of the upper atmosphere—dominated by the ionosphere, where ubiquitous free electrons and ions give precedence to electromagnetic effects—one wonders whether such layers stand as physically relevant to climate change as experienced near the Earth's surface. The WACCM attempts to affirmatively resolve this question. The most recent update, Version 6, as detailed by Gettelman et al., links various surface-level and tropospheric events to the general meteorological and chemical states of the upper layers [18]. Although the primary model, WACCM6, profiles only up to altitudes around 150 km, a variant, WACCM-X, extends the range to 500 km, thereby enabling consideration of JRO-relevant ionospheric processes. Regardless of the specific model employed, simulating the *effects* of whole-atmospheric processes confines one to those of the stratosphere and above. That is, the WACCM seems to effectively parameterize upper atmosphere values given lower atmosphere phenomena (e.g., examining the effects of volcanic eruptions on stratospheric wind patterns and ozone concentrations). However, it generally fails to perform the inverse operation: correlating upper atmospheric phenomena with surface datapoints.

Indeed, this discrepancy embodies one objective of I. Cnossen, who attempts to link tropospheric climate change to that of the upper atmosphere using successive iterations of the WACCM-X [19]. The author first highlights the physically manifested discrepancy of a cooling trend in the upper atmosphere—despite an opposite pattern observed near the surface. Cnossen acknowledges the known effects of ozone and greenhouse gas concentrations on the upper atmosphere’s cooling but notes that existing simulations often exclude the effects of “solar and geomagnetic activity.” The simulation timeframe encompasses the 1950-2015 period; subsequent regression analysis yields both spatial and temporal variations in several quantities—of which temperature at a 400 km altitude, geographically mapped and presented on a per-decade basis, stands as the most relevant. The purported connection between the troposphere and the upper layers comprises an auxiliary question of Cnossen; however, comparatively analyzing the important datapoints, *ceteris paribus*, yields a “negligible” correlation between the separate—even indirect—climatic effects of the lower and upper atmosphere layers.

The nature of the WACCM and the results of Cnossen’s simulations suggest that any scientific connection between tropospheric climate change and upper atmospheric phenomena, including electromagnetic anomalies in the ionosphere, still eludes definitive establishment. Despite the insight that JRO and similar experiments offer—and carry the potential to offer respecting the Earth’s surface—the urgency associated with the global climate change problem, manifested by increasingly demanding needs of rural Andean communities, warrants a shift of focus to direct, *in situ* observations of lower atmosphere effects. Among a vast, worldwide network of ground-based sensors, the conveniently located Huancayo Observatory serves this very purpose.

Huancayo Observatory

The Huancayo Observatory (HYO) sits approximately ten kilometers west of the namesake city. On the observatory grounds, the IGP operates ground-level and small radar instruments conducting real-time measurements of several climate-related variables. A brief review of the most relevant HYO sensors, followed by sampled assessments of their testing and deployment, serves to evaluate HYO's efficacy in executing much-needed climate studies for nearby agricultural communities.

Gradient Tower: The gradient tower stands above all other instruments on the HYO premises; it incorporates meteorological sensors at six distinct height levels: 2, 6, 12, 18, 24, and 29 m above the ground [20]. Among other measured variables, temperature and relative humidity constitute the tower's main data points of interest. A data logger positioned slightly below the first height level records such data points continuously at one-minute intervals.



Figure 13: Gradient Tower at HYO, measuring temperature and relative humidity

Averaging the temperature and humidity values among the six height levels allows one to assess the general short-term meteorological, or long-term climatic, state of the area surrounding HYO. According to the Director of HYO, José Flores, the observatory—despite publishing its instrumentation data through various studies—currently lacks a means of more specialized data analysis, including regression for more than one variable. A multi-purpose Python script accomplishes this; pulling from the gradient tower datasets, the program averages the six temperature and humidity data points—observed at each measurement time—and further decreases the resolution from one minute to 30 minutes for clarity purposes. The user selects

between separate temporal analyses and correlation analysis, manifesting themselves as dual line graphs and a temperature-to-humidity scatter plot, respectively, produced via the Matplotlib library. Figure 14 displays both graphical analyses for the gradient tower data collected throughout July 2022.

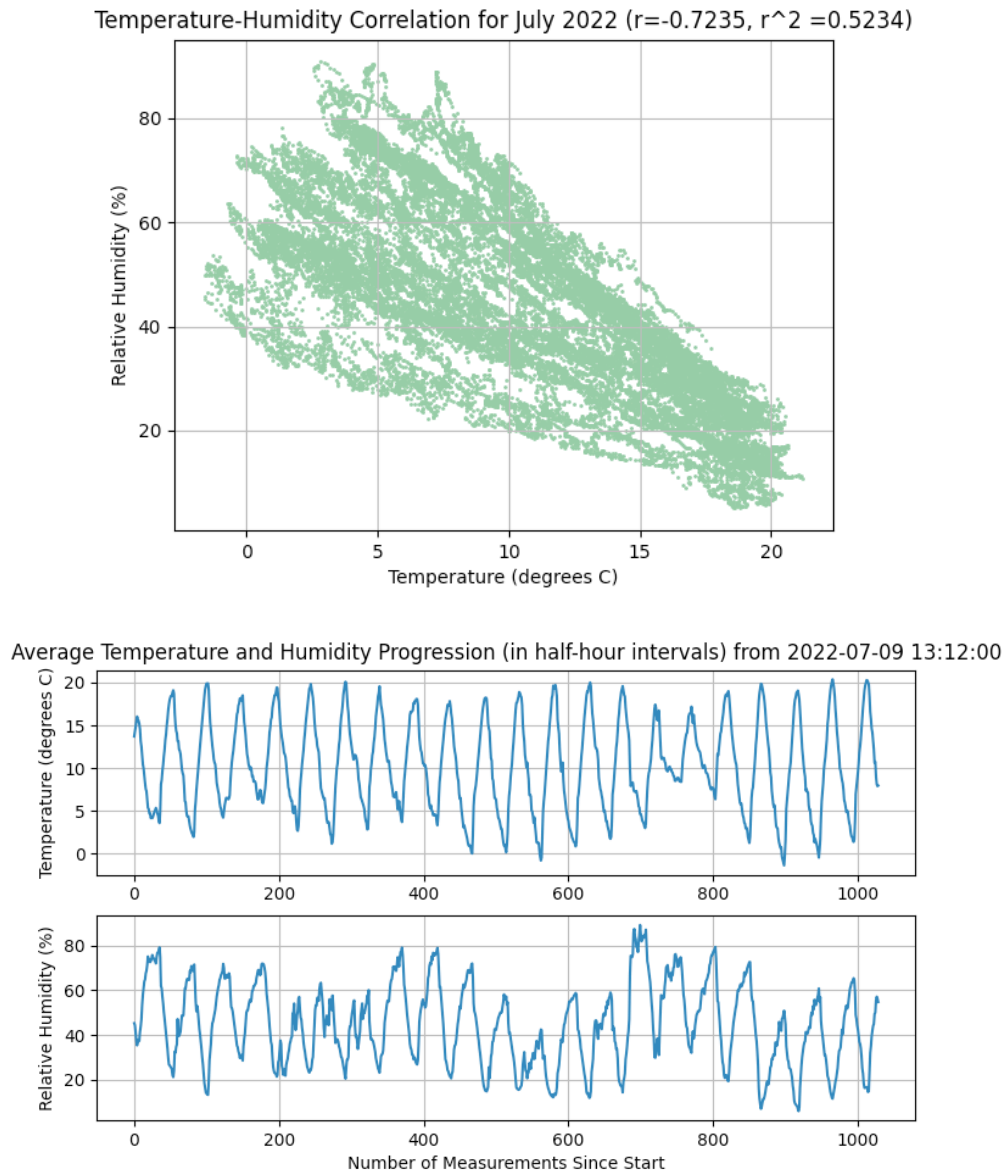


Figure 14: Correlative (top) and temporal (bottom) analyses for temperature and relative humidity during July 2022 (Data obtained from [21])

Repeating this for additional months—the measurements for which the HYO dataset makes readily available—yields a better understanding of the areal climate profile, specifically respecting temperature and relative humidity for a more pronounced time period. Additionally, performing comparative analysis on the six height levels of the gradient tower bestows such temperature and humidity measurements with a usually lacking vertical spatial resolution.

Black Carbon Analyzer: Among the most intently studied variables at HYO manifests itself not as a specifically “meteorological” parameter, but still as one that greatly concerns global climatologists: black carbon. The soot-like material emitted from most fuel-burning sources comprises a significant fraction of particulate matter (PM) in the lower atmosphere. Increased quantities of PM directly harm local air quality, leading to respiratory illnesses that often arise inexplicably in developing rural communities like Sicaya and Huayao [22]. Figure 15 photographs HYO’s black carbon analyzer, the Magee Scientific A33E-7, along with the external sensor that samples the surrounding air.

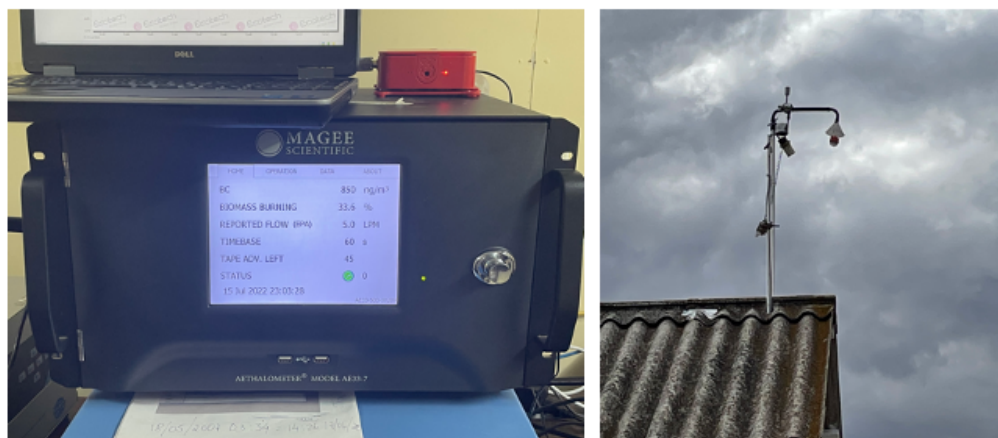


Figure 15: HYO black carbon analyzer (left) and external sensor (right)

Long-term studies of black carbon seek to determine its effects on the Huaytapallana Glacier, located approximately 40 km northeast of HYO. The glacier sits around 5000 m ASL and acts as the primary freshwater supply for several nearby communities, including the village of Hacienda Acopalca.



Figure 16: The Huaytapallana Glacier, as photographed from HYO on 30 June 2022

Residents in the immediately surrounding area attest that the glacier has been melting at an alarmingly fast rate over the past few decades. Further recession threatens to compromise the source of freshwater for Hacienda Acopalca and adjacent villages. In a coincident research study, Wilnelia Barea demonstrates the extent of black carbon deposition on the Huaytapallana Glacier by observing aerosols—fine particles suspended in the lower troposphere—within a 25 km radius of the glacier [23]. The author harnesses data obtained from a network of sun photometers, one of

which resides at HYO (Figure 17). Barea argues that the mass burning of trees in the Amazon region to the east, coupled with easterly trade winds transporting atmospheric particles from the Peruvian jungle region to the highlands region, constitutes the main source of the aerosols. According to the findings, a noticeable temporal decrease in snow “depth and density” implies the tendency of black carbon particles to settle on the glacier. Considering the long-term measurements produced by the sun photometer network—yielding aerosol optical depths that proportionally correspond to concentration values—and HYO’s on-site black carbon analyzer allows future researchers to more fully and accurately correlate aerosol incidence with black carbon concentration.



Figure 17: Sun Sky Lunar Multispectral Photometer CE318-T installed at HYO

Multi-Purpose Weather Station: Complementing the gradient tower, albeit at a singular fixed measuring height of 2 m above the ground, the HYO weather station comprises a Campbell Scientific METSEN500 Compact Weather Station that measures the following variables: temperature, relative humidity, barometric pressure, wind speed, and wind direction. The instrument connects to a Campbell Scientific CR310 Datalogger and a 12 V, 18 Ah lead-acid battery progressively charged by an external north-facing solar panel. Figure 18 photographs the sensor along with its auxiliary components as they currently sit on HYO premises.



Figure 18: HYO weather station (left) along with its data logger, power supply, and solar battery charger

The values outputted by the weather sensor sufficiently characterize the real-time meteorological state of the respective area. Aggregating such variables over extended time periods—as the HYO accomplishes through continuous monitoring—carries the potential to sufficiently characterize the corresponding climatic state, as well, respecting the most “sensory” of all measurable atmospheric data points.

Air Quality Monitor: When coupled with the aforementioned black carbon analyzer, HYO's Grimm Portable Dust Monitor more completely quantifies the state of air quality in the immediately surrounding region. Housed inside a stationary radiation- and precipitation-resistant shield (as shown in Figure 19), the sensor displays real-time mass concentrations of PM_{2.5} and PM₁₀, corresponding to dust particles of diameters less than 2.5 μm and less than 10 μm , respectively. The tendency of farmers in both Sicaya and Huayao—as evidenced by residents' direct testimony—to ignite controlled field fires motivates one to consider the effects of such fires, and their naturally occurring counterparts, on the local air quality; as demonstrated by Jaishree Gupta, Junín region air quality degradation remains conducive to poor respiratory health [22]. Specific, targeted research employing the HYO dust monitor serves not only to better characterize the region's air quality but also to enable observation of air quality trends as local communities modify their agricultural practices.



Figure 19: Grimm Portable Dust Monitor installed at HYO

Radar Instruments and Radiation Devices: Like the Jicamarca Radio Observatory, HYO incorporates several antenna arrays—in addition to a parabolic dish. The substantially lower operating power and collection area of such instruments, relative to the main JRO array, limits HYO radar-based studies to altitudes below 15 km. Three such radar apparatuses comprise Figure 20; utilized in conjunction with one another, they bestow researchers with valuable meteorological and atmospheric information not directly accessible via ground-level in situ measurements. Additionally, a 6 m-high tower consisting of three interdependent radiation sensors—a CMP10 Pyranometer measuring diffused solar energy, a CHP1 Pырheliometer measuring direct solar energy, and a CGR4 Pyrgeometer isolating the infrared (IR) component of solar radiation—assesses the extent of solar energy flux incident upon HYO [20].



Figure 20: HYO radar and radiation devices (clockwise from top left): Boundary Layer and Troposphere Radar (BLTR); Ka-band Doppler radar MIRA-35c; radiation instrumentation tower; rainfall estimation radar

Ozone Monitors: Completing the set of relevant in situ devices, two separate ozone (O_3) monitors reside near the black carbon analyzer. A Thermo Scientific 49i and a Model 41M, shown in Figure 21, measure quantities of tropospheric ozone near HYO. The Model 41M instrument harnesses ozone's absorption behavior, sampling a portion of the air with generated ultraviolet (UV) radiation and yielding the ozone concentration from the amount of radiation absorbed.



Figure 21: Thermo Scientific 49i and Model 41M ozone analyzers at HYO

Concentrations of ozone near the surface remain comparatively negligible in relation to stratospheric ozone, rarely exceeding 100 parts per billion (ppb) even in the highest-concentration regions [24]. Nevertheless, measuring ground-level ozone in a country like Peru enables one not only to fully profile regional air quality, but also to understand the extent of tropospheric ozone

production, depicted in Figure 22. The concentration of tropospheric ozone correlates with that of its heterogeneous reactants—primarily nitrogen oxide (NO_x) and volatile organic compounds (VOCs)—to a greater extent than that of its stratospheric counterpart. Because such compounds act as lower atmosphere greenhouse gases, fully understanding their formation—the potential for which the HYO ozone instruments offer—constitutes the first critical step toward implementing climate change mitigation efforts regarding tropospheric ozone.

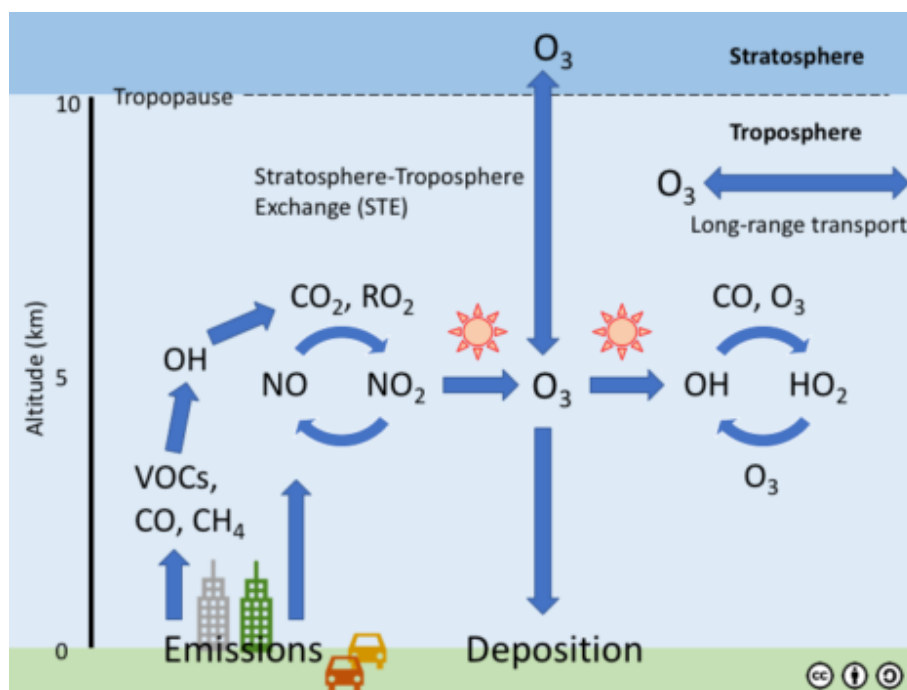


Figure 22: Tropospheric ozone production cycle (Source: [25])

Other HYO Instruments: Several other in situ and radar devices reside at HYO; Flores-Rojas et al. detail them in a comprehensive extreme weather events study [20]. The authors enumerate the specifications of the relevant instruments and justify each one's use in surveying three classes of extreme events: intense rainfall, intense frost, and high pollution. All stand as

relevant to the surrounding agricultural communities, including Huayao and Sicaya. Rainfall pervades the region during the wet season (December to March), unexpected frost—as noted by the residents themselves [14, 15]—devastate crops during the growing season, and aerosols—both naturally occurring and fire-induced—linger over the region and persistently affect the Huaytapallana Glacier, as demonstrated by Barea [23]. Extending beyond the instruments described here, Flores-Rojas et al. assess soil temperature and moisture in addition to daily rainfall totals with a rain gauge. Linking their quantitative results to observed events, the authors deduce a generally high degree of efficacy characterizing all HYO instruments they employ. They further claim that such instruments offer to preemptively assist local agricultural communities by contributing to local climate model development and extreme weather event prediction.

Other published HYO studies relate more specifically to comparative instrument testing procedures. Valdivia-Prado et al. test ten sets of identical instruments installed at HYO [26]. The authors compare each measured parameter group (including temperature, relative humidity, pressure, rainfall intensity, and raindrop size) against one of two datasets: corresponding accepted mean values and measurements by other “conventional” meteorological sensors. Generally, the instruments behave according to expectation—with determination coefficients rarely falling below 0.90. For some parameters (most notably wind speed and raindrop size), a few sensor groups yield significant outliers or correlations contrary to conventional measurement. Citing lack of relevant manufacturer information, the authors point toward further evaluation and testing in the future. Statistical analysis constitutes the primary focus of the paper; however, the study fails to address possible applications or deployments of the tested sensors outside HYO.

Such a shortcoming highlights the primary limiting factor of instruments at HYO or at any similar observatory throughout the world: their fixed positions. Although a sufficiently high

temporal resolution characterizes most in situ measurements—sometimes in one-minute intervals, necessitating an intentional resolution degradation to display the Figure 14 data—the devices’ stationary nature confines the spatial resolution to the radial distance between one instrument and its nearest counterpart. Within Peru and other developing nations, the distribution of sensor networks remains relatively sparse. While some variables still adequately characterize a large area—e.g., the Junín region—at low spatial resolutions, others, such as particulate matter concentration, directly affect communities at the household and even individual level. Even a fixed network of air quality monitors fails to adequately pinpoint the health and climatic impacts of small-scale events, such as local field fires, and individuals’ habits like biomass cooking. Moreover, the residents of Sicaya and Huayao expressed general desire to more fully understand weather events and climate patterns at the community level. Herein lies the motivation to review studies incorporating portable sensors, thereby achieving the spatial resolution sought by global climatologists and local Andean residents.

Reviewing Previous Portable Instrumentation Studies

Beyond HYO—and beyond the borders of Peru—various projects implement mobile meteorological sensors for climate-focused studies. One such investigation entails Wildmann et al. deploying a glider on 30 flights in the Southern Andes region to evaluate tropospheric winds [27]. The payload includes standard meteorological instruments—temperature sensors, a relative humidity sensor, a compass and a global positioning system—along with a three-axial wind probe. The paper heavily focuses on detailing the experimental setup and the associated physics in order to convey its optimization. Although the ‘Results’ section provides wind speed distribution plots

(which embody the study's primary objective) and sensor performance analysis, it fails to contextualize the full parameter set to a broader research question. Instead, the authors extend their discussion of the experiment design to suggest further improvements, only briefly acknowledging the study's relevance to Andean aircraft (e.g., glider) operators. Despite these shortcomings, the investigation demonstrates the feasibility of airborne in situ measurements and motivates one to orient similar experiments to more general and meaningful research questions.

On a smaller scale, yet with a more systems-based approach, Arghirescu et al. design a portable sensing system that employs an Arduino microcontroller architecture and attaches to a remote-controlled drone or boat [28]. They begin by discussing their motivation—the need to further autonomize field-deployed sensor networks—and reviewing existing implementations and engineering methods. Addressing the shortcomings of each design (and conceding their chosen microcontroller's shortcomings), the authors justify incorporating auxiliary components—most notably the higher resolution analog-to-digital converter (ADC)—to keep their solution as reliable yet power- and space-efficient as possible. Electrical schematics and pseudocode algorithms follow; both encompass data acquisition via the external ADC, monitoring via light-emitting diodes (LEDs), and correction via a relay. Despite providing photographs of final construction and implementation (showing the circuit on the vehicular bodies), the authors mainly confine testing to basic current measurements; they even deem the rather low ammeter values not commensurate with actual system deployment. Although the authors offer design solutions to address the high power consumption (e.g., inserting a current-tolerant buck converter) and enumerate further system benefits, the paper lacks a comprehensive assessment of the network's field performance, and the general phrase “cities or protected nature reserves” fails to convey specific testing and deployment locations.

In perusing the existing literature related to Andean climate change studies, one discovers several experiments dedicated to characterizing local air quality. This exemplifies itself no better than in a study by Nicolaou et al., who detail an investigation into the health effects of biomass-caused particulate matter (PM) in rural Puno, Peru, located in the southern highlands region [29]. The authors set up experiments in 20 households not only to assess particle species and concentrations (resultant from twice-daily cooking) but also to determine respiratory impacts from exposure. Through intra-household temporal distribution plots and lung deposition histograms, the study demonstrates that Puno residents—particularly the women who regularly cook—experience average daily exposures substantially greater than the World Health Organization (WHO) suggested limit. In fact, the authors synthesize their study with those researching smokers to convey the problem’s severity. Other than providing a brief experiment description, the paper refrains from assessing instrument performance, instead focusing on the measurement results. Moreover, although they cite similar studies, the authors fail to address the means of repeating the main experiment in other Andean communities; they confine “future work” statements to examining what they term “inter-subject variability” regarding lung depositions.

Additionally, Kephart et al. almost identically mirror the Nicolaou et al. project monitoring the effects of cooking-induced PM_{2.5} in rural Puno, Peru, only deviating to focus instead on nitrogen dioxide (NO₂) concentrations and residential women’s personal exposure to the gas [30]. The researchers set up both passive and active measuring devices—including wearable Ogawa Passive Samplers—in 100 household kitchens and monitor each one over a 48-hour period. For the 97 successful measurements (three discarded due to battery failure), Kephart et al. find substantial average NO₂ concentration spikes during the two hours following 06:00 PET and 18:00 PET; in fact, around 8:00 PET, 60% of sampled kitchens exhibit concentrations at or above the

“WHO indoor hourly guideline of 163 ppb.” Furthermore, 91% of the kitchens experience such maximum concentrations at some point during the study. The authors acknowledge the project’s shortcomings—ranging from the relatively small sample size to the potentially confounding high altitude of Puno—but note that their study constitutes one of the first to directly assess NO₂ kitchen concentrations and personal exposure levels in such a community.

Yet another study bridges PM and climate-related variables to assess instrument performance in Lima, Peru. Romero et al. focus on developing a multiple linear regression model (MLRM) to relate air quality measurements to standard meteorological parameters in the city [31]. Specifically, the authors attempt to establish the mathematical relationship between both classes of PM concentrations (PM_{2.5} and PM₁₀) and temperature and relative humidity. They deploy a low-cost but stationary PurpleAir sensor in the Jesús María district of Lima for three weeks in October 2019 and compare its measurements of the four aforementioned quantities to those between two reference stations. In conducting the experiment, Romero et al. convey the effectiveness and efficiency of low-cost particle concentration sensors in developing nations like Peru. They discover positive correlations between the meteorological parameters and particulate matter concentrations—with a notably stronger correlation exhibited for PM₁₀. The authors establish temperature as the more influential of the two meteorological parameters; also, they qualify the PurpleAir sensor’s “high performance” with observed strong correlations between the PM measurements and those from the reference station. Similar studies carried out in the rural areas of Peru offer the potential not only to fully characterize the country’s air quality, but also to understand personal PM exposures in limited-access communities by magnifying the spatiotemporal resolution via a portable sensor network.

Despite the paramount importance of the previously discussed parameters, no assessment of climate change stands complete without assessing the phenomenon's most palpable cause: greenhouse gases. Hwang et al. employ a portable carbon dioxide (CO₂) sensor to study the correlation between CO₂ concentrations and the amount of “carbon stock”—i.e., features characterized by their absorption of CO₂, such as forests—defining the area [32]. They aim to establish a link between in situ CO₂ values and the specific conditions of the region under question (e.g., forest density and vegetation age). The authors focus on a wooded area near Yuga-Myeon, South Korea, in which they conduct measurements at 182 distinct points. Expecting to discover a reliably negative correlation between carbon stock and local CO₂ concentrations, Hwang et al. actually produce inconsistent results whereby a relatively high CO₂ concentration value sometimes defines a dense forest area. They conclude that topographical features—even those independent of the amount of forestry—substantially influence the sensor's performance; this calls for additional in situ CO₂ tests of different terrains with different instruments to determine the validity of the authors' claim.

Chapter 3

Designing a System for Andean Communities

As evidenced by the above review, numerous portable measuring systems exist, and many show promise of reliability in effectively studying both climate change and air quality dynamics. However, assessment of the Peruvian Junín region in particular stands limited to stationary HYO instruments. Meeting the needs of surrounding communities, exemplified by the testimony of Huayao and Sicaya residents, warrants improving spatial resolution to the order of several meters to quantify the effects of global climate change (and of peoples' adaptations to it) at the household level. A portable, independently powered system integrating both meteorological and air quality instruments—one that enables both spatial and temporal measurements—fits this objective.

Design Principle

The foremost consideration for designing such a sensor network manifests itself as the 'citizen science' tenet. While published, credibly verified research studies comprise an indispensable part of regional climate-related knowledge, direct knowledge by immediate stakeholders, the affected people, remains equally important. Therefore, any instrumentation system's design should facilitate use by non-engineers and non-scientists making up the relevant communities. Simplifying the interface and choosing an easily learnable, open-source onboard control module accomplishes this end.

Additionally, maintaining the 'portable' and 'user-friendly' attributes of the proposed system relies on restricting the devices' weights and maximizing the ability to transport them. This entails choosing sufficiently light components and physically integrating them such that hand or

vehicle carriage remains feasible. Simultaneously, remotely deploying the sensors—in often isolated locations—necessitates system durability against precipitation; after all, ‘extreme weather events’ form the very bases for conducting research. Enclosing all sensory, control, and power components in a handheld waterproof container protects the physical integrity, and thus performance, of the system.

The design must also weigh the expectation that a single system lacks the ability to adequately survey all localities that require assessment. While the central Andean communities of Sicaya and Huayao—more specifically, their residents’ testimonies—comprise the motivation for conducting this specific project, the small-scale nature of potential deployments warrants system replicability and, therefore, low cost. Selecting a relative handful of physically small in situ instruments (as opposed to inevitably costly and bulky radar and remote sensing devices) not only facilitates deployment as previously addressed; it also catalyzes the establishment of a regional, a national, or even an international network of meteorological and air quality sensors. Each individual system, while characterized by the same design principles enumerated above, tailors to the specific needs of the region in which one deploys it. Likewise, the substantial coverage bestowed by replication and selective geographical positioning stands to aggregately provide a large-scale, possibly global, understanding of climate and air quality trends. Considering the potential for cost efficiency and modified duplication, therefore, bolsters climate-related knowledge unique to each of numerous diverse communities while reinforcing and confirming the general patterns that have collectively comprised the subject of studies for decades.

In accordance with such principles, the following sensory and auxiliary components make up the system proposed for testing and deployment in Sicaya and Huayao of Peru’s Junín region.

System Components

As noted in Chapter 1, ten anonymous residents of Huayao describe their experiences with extreme temperatures, particularly those approaching -20°C . Of particular interest is one resident's observed discrepancy whereby a temperature of -18°C (as measured by IGP instruments) "feels warmer" than a temperature of -5°C [14]. While the dual effect of humidity on one's perceived sensational temperature establishes itself as accepted knowledge, the testimony nevertheless conveys the need for localized, mobile sensing within Huayao. A system reserved for deployment within the community not only allows for constant monitoring but also enables nearly ideal spatial resolution—i.e., down to the household level.

Moreover, the prevalence of harmful PM in Andean communities—as exemplified by Nicolaou et al. in Puno [29]—bolsters the case for more regular and frequent monitoring in Huayao and Sicaya. Household measurements over time enable one to correlate changing PM exposure levels with occupants modifying their habits. For example, partial or full adoption of solar cooking—as described by Tarang Shah [33]—may constitute temporal decreases in PM concentrations to a salubrious effect. Measuring particle size distribution (smaller particles deposit in lungs more readily) and acquiring PM_{2.5} and PM₁₀ air quality reports comprehensively illustrate the individual states of exposure and, by consequence, health.

Finally, no complete atmospheric profile exists without measurements of the two most potent greenhouse gases: carbon dioxide (CO_2) and water vapor (H_2O). Numerous past studies demonstrate a strong correlation between atmospheric carbon dioxide concentrations and average global temperature, the defining parameter of climate change. Average CO_2 concentrations have exhibited positively linear trends over the past few decades, remaining on the order of 400 parts

per million (ppm) [34]. A sensor that encompasses this magnitude—and the corresponding value for water vapor—would be effective in remote surveying.

The preceding information justifies the need for assessing five specific parameters: temperature, relative humidity, PM (both concentration and size distribution), CO₂ concentration, and H₂O concentration. The subsections below detail the chosen instruments and the accompanying data logging and power systems.

Temperature and Humidity Probe: Since climate change manifests itself as bilateral extreme temperatures, employing a highly value-tolerant sensor stands as an engineering sine qua non. Moreover, the ability to survey the entire relative humidity range (0% to 100%) enables one to statistically relate community members' observations—e.g., the aforementioned sensational temperature discrepancy—to actual measurements. The RM Young 41382VC Relative Humidity/Temperature Probe, which outputs two voltage signals corresponding to temperature and relative humidity, fits such requirements. The 41382VC sensor's physical packaging and quantitative specifications comprise Table 2.

Table 2: 41382VC Probe image [35] and specifications [36]



INSTRUMENT	Temperature/Humidity Sensor - Young Model 41382VC
COST	\$858.00
SHIPPING TIME	3-4 weeks
POWER REQUIREMENTS	Input Voltage: 8-30 VDC @ 7mA
MEASUREMENT INTERVAL	10 seconds
DATA LOGGING	External
MEMORY	/
RESOLUTION	Temperature: Within 0.3C Humidity: Within 1% RH
RANGE	Temperature: -50C to +50C Humidity: 0% to 100% RH
DIMENSIONS	18.8 x 6.2 x 6.2 cm
WEIGHT	<0.5kg
DATA OUTPUTS	0-1 VDC or 0-5VDC signal
BAUD RATES	/
WARRANTY	One year

Particulate Matter (PM) Counter: Particulate matter affects public respiratory health more immediately and noticeably than most gas species. Understanding particles' identities—examples of which are dust, pollen, combustion particles, and organic compounds—and their spatial and temporal behavior enables assessment of public health due to pollution.

The large radial size of pollution particles also distinguishes them from the gases, which are all molecular units. Most particles are on the order of either $<10\mu\text{m}$ or $<2.5\mu\text{m}$, rarely exceeding $10\mu\text{m}$. Identifying and parameterizing particulate matter, therefore, begins with measuring particle sizes.

The Handilaz Mini II Particle Counter from Particle Measuring Systems comprises the means for quantifying PM sizes. Characterized by a size range of $0.2\ \mu\text{m}$ to $10\ \mu\text{m}$ and a resolution of $10\ \text{nm}$, the Handilaz device employs a rechargeable lithium-ion battery and independent Secure Digital (SD) data storage. The primary operating modes stand as follows: finite particle sampling (whereby the sensor takes in a fixed number of in-range particles and textually maps the size

distribution) and air quality analysis (whereby the device generates both quantitative and qualitative PM2.5 and PM10 reports). Table 3 photographs the instrument and tabulates its specifications.

Table 3: HandiLaz Mini II Particle Counter image [37] and specifications [38]



INSTRUMENT	HandiLaz Mini II Particle Counter
COST	\$4,400.00
SHIPPING TIME	4-5 weeks
POWER REQUIREMENTS	User-replaceable Li-Ion Battery 5 hr cont., 10 hr intermittent counting
MEASUREMENT INTERVAL	?
DATA LOGGING	USB or SD Card
MEMORY	/
RESOLUTION	10 nm particle size
RANGE	0.2-10 um particle size
DIMENSIONS	8.2 x 13.7 x 4.2 cm
WEIGHT	0.83 kg
DATA OUTPUTS	SD data lines
BAUD RATES	/
WARRANTY	One year

Carbon Dioxide and Water Vapor Analyzer: The instrument chosen for the Central Andes study is the LI-COR Biosciences LI-850 Gas Analyzer. It accepts 12-30 VDC power and harnesses a pump-filter combination to output a 0-2.5 VDC or 0-5 VDC signal for each parameter. Like the temperature and humidity sensor, the LI-850 relies upon an external data logging module; thus, the direct real-time software interface becomes obsolete for remote surveying. This device considerably outweighs the other sensors, as the relevant specification indicates in Table 4.

Table 4: LI-850 Gas Analyzer image [39] and specifications [40]



INSTRUMENT	LI-850 CO ₂ /H ₂ O Analyzer (with display and pump)
COST	\$6,574.00
SHIPPING TIME	/
POWER REQUIREMENTS	Input Voltage: 12-30 VDC 0.42 A @ 12VDC (with pump) During warmup: 1.2 A @ 12VDC (maximum)
MEASUREMENT INTERVAL	0.5 seconds
DATA LOGGING	External
MEMORY	/
RESOLUTION	Within 1.5% of readings
RANGE	CO ₂ : 0-20000 ppm H ₂ O: 0-60 mmol/mol
DIMENSIONS	12.23 x 17.85 x 7.62 cm
WEIGHT	1.32 kg
DATA OUTPUTS	0-2.5 VDC or 0-5VDC signal
BAUD RATES	9600
WARRANTY	Two years

Data Logging Mechanism: While the particle counter retains an independent SD storage system, the temperature and humidity probe and gas analyzer require external data loggers for capturing the outputted voltages. Extracting the temperature and humidity values and gas concentrations then reduces to mapping each intermittent voltage to the corresponding quantities according to the Figures 23 and 25 specifications. The open-source Arduino Mega 2560 board serves as an effective microcontroller to achieve this end. Additionally, employing an Arduino controller—as opposed to a more robust research-grade device (e.g., the DATAQ Instruments Model DI-2108 Data Logger)—bolsters the ‘citizen science’ objective characterized by facilitated direct community use. The differential outputs from the 41382VC probe and LI-850 device collectively feed into six analog inputs (with a separate ground common to each instrument’s variables) while an SD card reader employs four digital inputs in conjunction with 5 V power. Figure 23 provides a system block diagram with an accompanying Arduino Mega 2560 photograph.



Figure 23: Data logging system diagram with Arduino Mega 2560 microcontroller

Power Supply: One primary challenge defines any remote sensing application: continuously supplying power to the active measuring devices. The term “remote”—in the context of Central Andean atmospheric profiling—implies no connection to wireless networks or grid power. Thus, not only must all data remain localized; the power supply must somehow draw from its sparse environment.

The aggregate specifications of two of the three chosen sensors (all except for the particle counter) indicate a common tolerable input voltage of 12 VDC. Also, the average current draw of each device yields an estimated battery capacity according to the desired recharge period. The component power requirements and the need to run the station for several hours at a time results in a necessary capacity of around 10Ah for a single battery.

Despite the 10Ah estimate, the risk of undercharging the battery (below the “safety factor” of roughly 20% capacity) warrants consideration of battery capacities above 10Ah. Three separate design options—along with their specifications—comprise Table 5.

Table 5: Specifications for three battery options

BATTERY	ExpertPower Lithium LiFePO4	ExpertPower Lithium LiFePO4	Nermak LiFePO4 Li-Ion Phosphate
		Quantity = 2	**Quantity = 2**
Voltage	12.8V	12.8V	12.8V
Capacity	20Ah	10Ah x 2	12Ah x 2
Terminal Type	M4	F2	F2
Dimensions	7.1 x 3 x 6.6 in	6 x 2.6 x 3.7 in (x2)	6 x 3.9 x 3.8 in (x2)
Weight	5.8lb	2.7lb (x2)	3.23lb (x2)
Cost	\$200	\$176 (total)	\$108 (total)

The significantly reduced weight of lithium-ion (Li-Ion) batteries with respect to their lead-acid counterparts renders Li-Ion a fitting choice for the power supply. Specifically, the low cost and the higher capacity (12Ah) of the Nermak Lithium-Iron-Phosphate (LiFePO₄) Battery renders the best choice among the three candidates. With two units employed in the station, one may recharge while the other operates.

Additionally, while the temperature and humidity probe tolerates such a DC voltage (specifically characterized by a range of 12 V to 30 VDC), the Arduino microcontroller requires either buck conversion or inversion to AC power. The nature of the system favors the latter; thus, a BESTEK 300 W inverter (12 VDC to 110 VAC) connects the supply battery to the Arduino via the controller's AC power cord. Because of the particle counter's existent onboard rechargeable lithium-ion battery and SD card support, the instrument stands independent of both the data logging system and the power system. One infers this by its absence from the complete station block diagram, which comprises part of Figure 24 below.

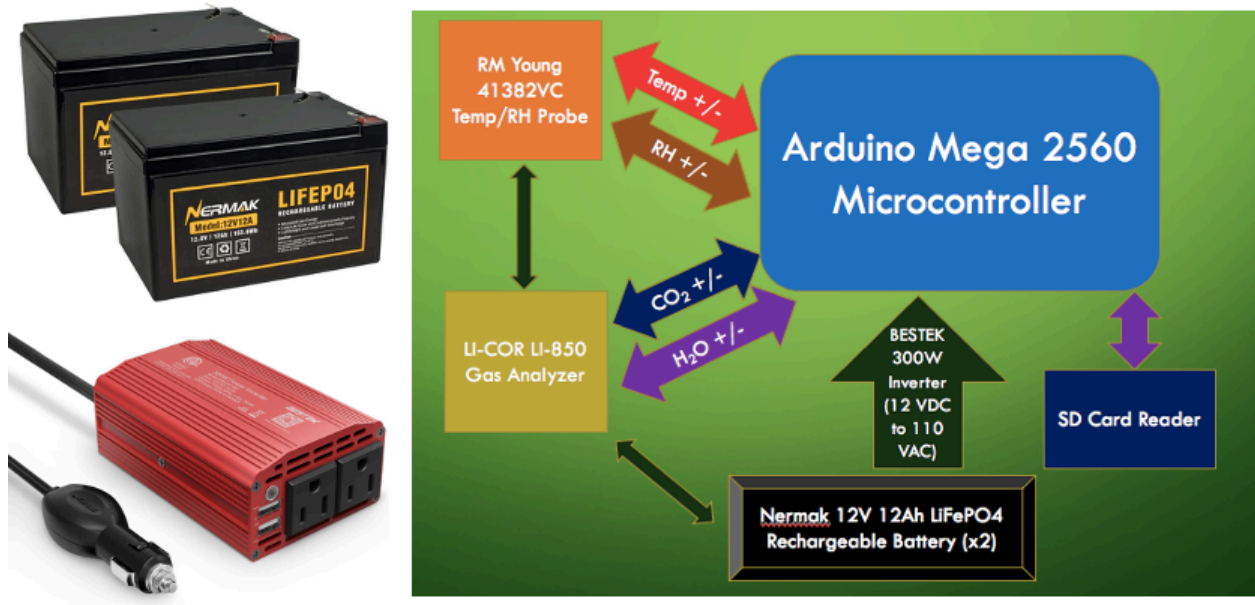


Figure 24: System diagram with LiFePO₄ battery [41] and DC-to-AC inverter [42] images

To accommodate extended remote site deployment, a SUNER POWER 12 V, 20 W Solar Battery Charger maintains either battery during sunlight hours. The principle behind this design facet derives from the main charging method employed at HYO, illustrated by the rightmost image of Figure 18. The high elevation of the Junín region—and all Andean regions—affords especially strong sunlight, thus allowing one to realize nearly the full power rating of 20 W. With the power capacity of each battery standing at 153.6 Wh, full sunlight conditions and proper, actively monitored panel orientation enable full charging of each LiFePO₄ battery in under eight hours. Moreover, despite a length of 52.7 cm defining its main dimension, the panel weighs 2.3 kg, facilitating direct hand carriage or temporary mounting by most users. An image of the chosen solar battery charger makes up Figure 25.



Figure 25: SUNER POWER 12 V, 20 W Solar Battery Charger [43]

Packaging: To shield the electronic components from sunlight and precipitation, two Gratury junction boxes house the instruments, the data logger, the active battery, and all auxiliary items. Both rated by the manufacturer as waterproof, the larger box and the smaller box measure at 400 x 300 x 180 mm and 290 x 190 x 140 mm, respectively; such dimensions account for the volume of each constituent part occupying a box during deployment. Figure 26 displays both Gratury boxes as photographed during the initial testing stage.



Figure 26: Photographs of larger (left) and smaller (right) Gratury junction boxes

Determining the efficacy of the aforementioned design requires procedural testing of the individual components, detailed in the following chapter.

Chapter 4

Conducting Initial Testing

The need for effective initial testing on such a multi-faceted subsystem warrants specific assessments of each of the three subsystems: the sensors, the data logger, and the power supply. Extenuating circumstances precluded broad and comprehensive testing during the course of the visit to Peru and in the months thereafter; in fact, only experiments conducted with the particle counter stand reminiscent of a system ‘deployment.’ Nevertheless, verifying the performance and operational facility of the remaining components provides insight into the entire system’s feasibility for total deployment. The following sections describe such verification for each enumerated subsystem.

Sensor Testing

This stage entails separate testing procedures for the particle counter, the temperature and humidity probe, and the gas analyzer. Each device’s small-scale experiment conveys the feasibility of longer and more substantive operations by the aggregate system. The proceeding subsections present the tests’ circumstances, any analysis-facilitating software, and the acquired graphical data.

Particle Counter: On 19-20 July 2022, a substantial mountainside fire burned approximately 3 km southwest of HYO. Figure 27 provides a photograph of the fire, taken at 18:59 Peru Time (PET) on 19 July.



Figure 27: Large fire near HYO (photograph taken at 18:59 PET on 19 July 2022)

Because Central Andean mountainside fires and field fires occur quite frequently during the dry season—which the month of July comprises—quantifying fires’ effects on PM remains of high research importance [12]. Comparatively measuring PM size distribution and mass concentration before and after such events allows one to probabilistically attribute any discrepancies to the fires.

Figure 28 shows a labelled map of HYO. At each of the four marked points, the Handilaz Mini II Particle Counter measures average particle size distribution and mass concentrations (for both PM_{2.5} and PM₁₀)—once on 18 July (before the aforementioned fire) and again on 20 July (after the fire).



Figure 28: Satellite image of HYO with the four labelled test sites [11, 44]

For both particle size distribution and mass concentration, the particle counter stores the data in textual log files. As listed in Table 3, the particle size resolution stands at 10 nm (0.01 μm). A Python script—integrating the Matplotlib library—converts the numerical size counts into a normalized distribution over the entire size range (0.20 μm to 10.0 μm). Each graph displays the measurement timestamp (in local Peru Time) and the number of particles sampled to constitute the statistical bars. Figure 29 illustrates an example of this programmatic transformation; it depicts a preliminary measurement carried out on 8 July 2022.

Date&Time: 070822-130609
 Elapsed Time: 00:03
 Temp: 21.6C
 Pressure: 69.0 kPa
 RH: 57.5

Size	Cum. Counts
0.20	20048
0.21	20007
0.22	19967
0.23	19905
0.24	19843
0.25	19793
0.26	19744
0.27	19692
0.28	19641
0.29	19588
0.30	19535
0.31	19473
0.32	19412
0.33	19346
0.34	19281
0.35	19271
0.36	19261
0.37	19161
0.38	19061
0.39	19000
0.40	18939
0.41	18884
0.42	18829
0.43	18780
0.44	18731
0.45	18678
0.46	18625

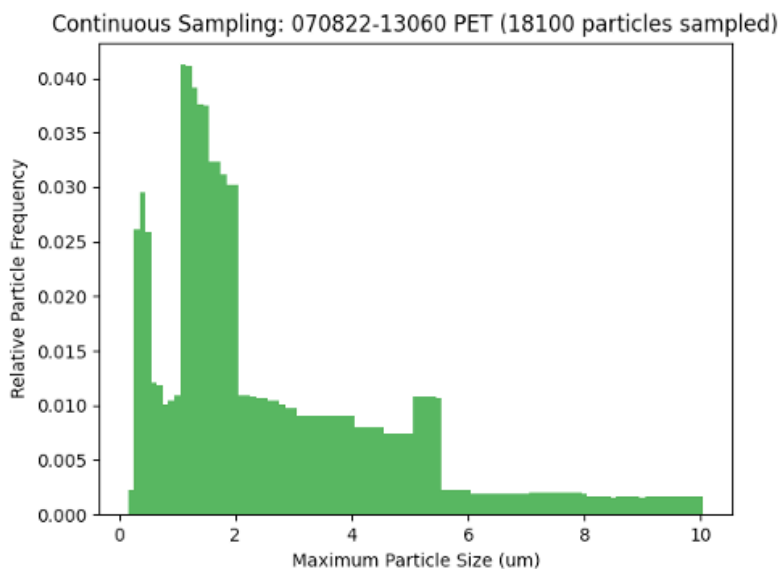
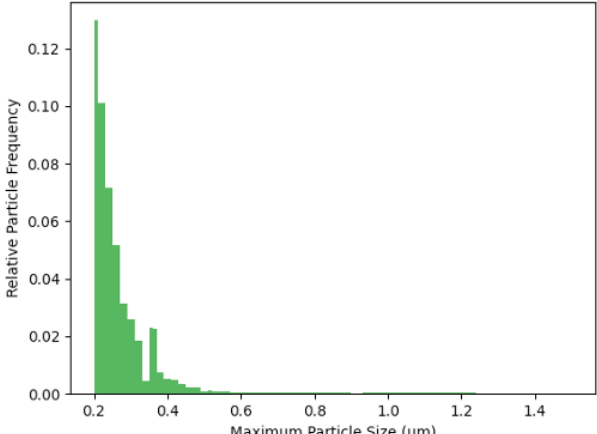
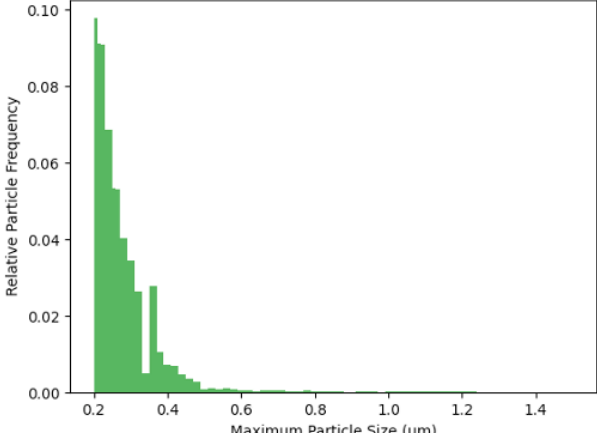


Figure 29: Sample illustration of log file conversion to size distribution plot

For the study under question, Table 6 enumerates the size distribution plots and PM mass concentrations for the four measurement sites (Figure 28) for 18 July; Table 7 repeats this for the post-fire experiment on 20 July. Due to the samples' extreme skews toward smaller particle sizes, the plots reflect a modification of the size range to [0.20 μm , 1.50 μm]. In each of the eight trials, larger particles (i.e., those with diameters exceeding 1.50 μm) exhibit aggregate counts less than 0.5% of the total number of sampled particles.

Table 6: Pre-fire PM measurements at four HYO test sites on 18 July 2022

SITE	TIME (18 JULY 2022)	PM2.5 AND PM 10 MASS CONCENTRATIONS	NORMALIZED PARTICLE SIZE DISTRIBUTION
1 (SW)	14:40 PET	<p>PM 2.5: 0.3 $\mu\text{g}/\text{m}^3$ (0.8% daily limit)</p> <p>PM 10.0: 8.4 $\mu\text{g}/\text{m}^3$ (5.6% daily limit)</p>	<p>Continuous Sampling: 071822-144007 PET (19927 particles sampled)</p> 
2 (SE)	14:47 PET	<p>PM 2.5: 2.6 $\mu\text{g}/\text{m}^3$ (7.4% daily limit)</p> <p>PM 10.0: 79.4 $\mu\text{g}/\text{m}^3$ (52.9% daily limit)</p>	<p>Continuous Sampling: 071822-144743 PET (19937 particles sampled)</p> 

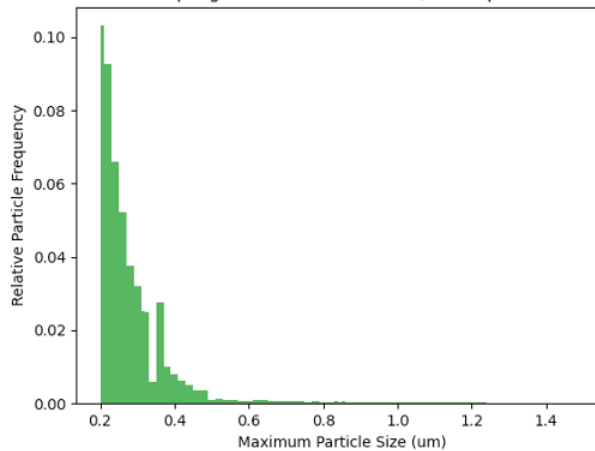
3
(NE)

16:23
PET

PM 2.5:
2.1 $\mu\text{g}/\text{m}^3$
(6.0% daily limit)

PM 10.0:
21.6 $\mu\text{g}/\text{m}^3$
(14.4% daily limit)

Continuous Sampling: 071822-162349 PET (19966 particles sampled)



4
(NW)

16:11
PET

PM 2.5:
2.3 $\mu\text{g}/\text{m}^3$
(6.4% daily limit)

PM 10.0:
16.9 $\mu\text{g}/\text{m}^3$
(11.2% daily limit)

Continuous Sampling: 071822-161101 PET (19973 particles sampled)

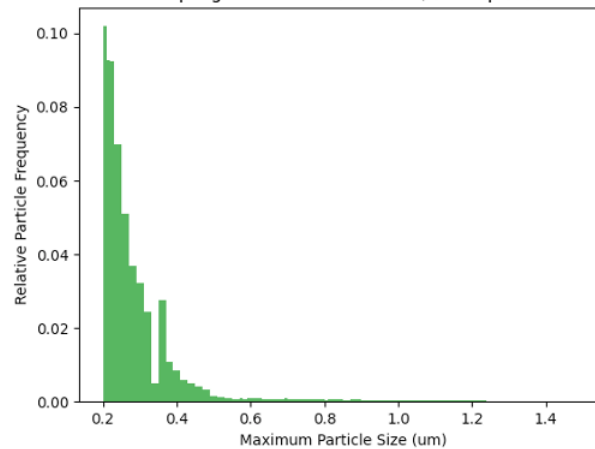
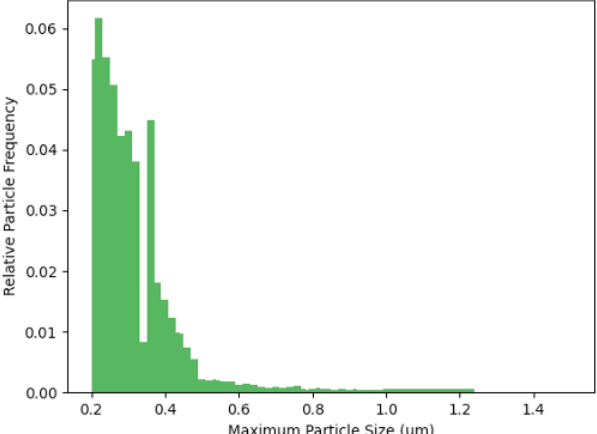
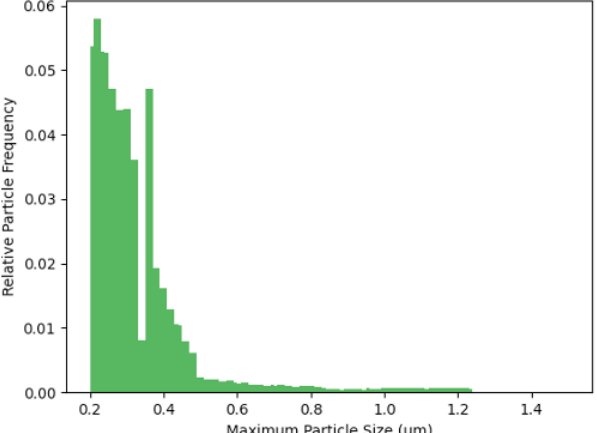


Table 7: Post-fire PM measurements at four HYO test sites on 20 July 2022

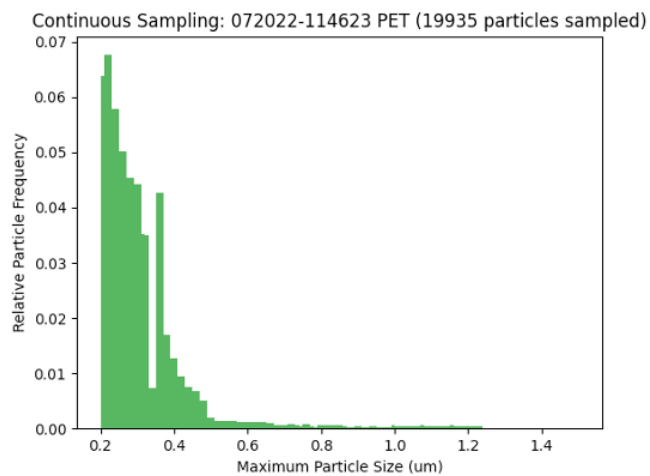
SITE	TIME (20 JULY 2022)	PM2.5 AND PM 10 MASS CONCENTRATIONS	NORMALIZED PARTICLE SIZE DISTRIBUTION
1 (SW)	11:25 PET	<p>PM 2.5: 4.7 $\mu\text{g}/\text{m}^3$ (13.5% daily limit)</p> <p>PM 10.0: 60.1 $\mu\text{g}/\text{m}^3$ (40.0% daily limit)</p>	<p>Continuous Sampling: 072022-112555 PET (19952 particles sampled)</p> 
2 (SE)	11:33 PET	<p>PM 2.5: 4.4 $\mu\text{g}/\text{m}^3$ (12.6% daily limit)</p> <p>PM 10.0: 67.2 $\mu\text{g}/\text{m}^3$ (44.8% daily limit)</p>	<p>Continuous Sampling: 072022-113351 PET (19935 particles sampled)</p> 

3
(NE)

11:46
PET

PM 2.5:
3.9 $\mu\text{g}/\text{m}^3$
(11.2% daily limit)

PM 10.0:
52.8 $\mu\text{g}/\text{m}^3$
(35.2% daily limit)

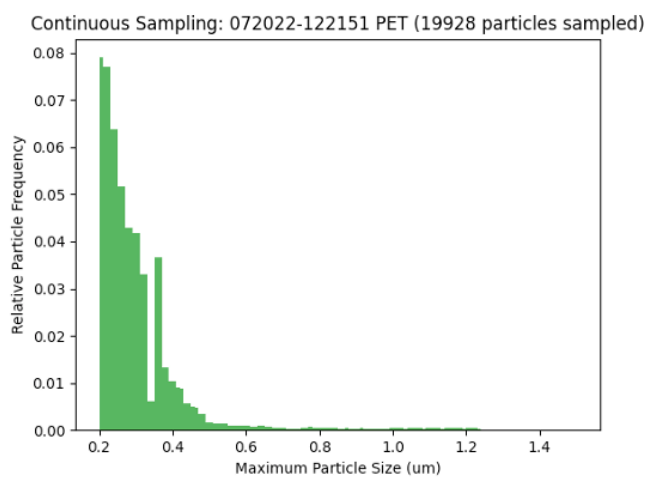


4
(NW)

12:15
PET

PM 2.5:
3.1 $\mu\text{g}/\text{m}^3$
(8.8% daily limit)

PM 10.0:
61.5 $\mu\text{g}/\text{m}^3$
(41.0% daily limit)



Temperature and Humidity Probe: Due to several hardware development issues related to the Arduino SD card reader, current implementation of the 41382VC probe in Peru remains limited to a 34-minute-long indoor test. Moreover, the test fails to encompass field deployment; the system rests atop a desk with the Arduino Mega connected to the computer—necessary due to the lack of an external data logging mechanism. Figure 30 photographs the setup for the test.

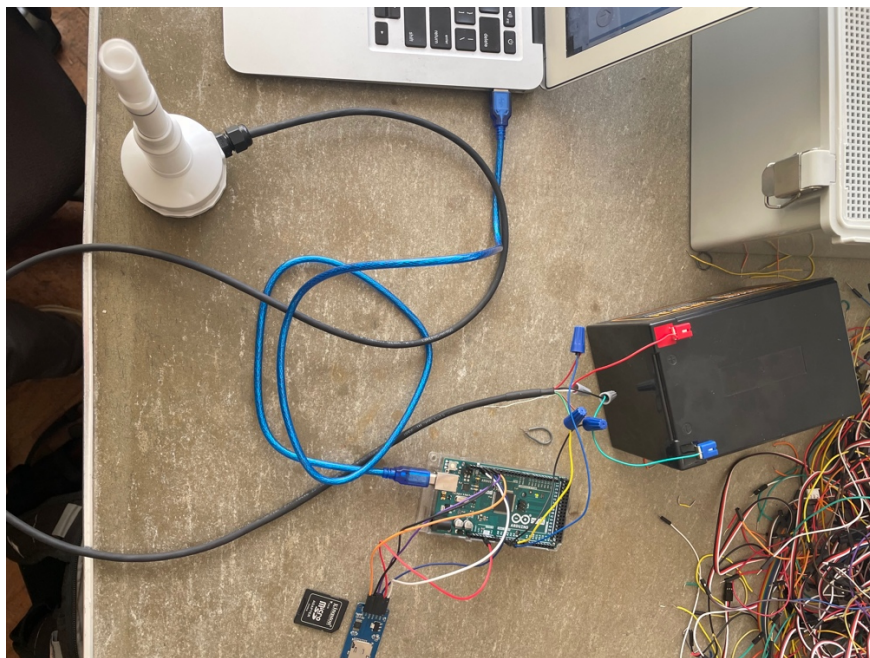


Figure 30: Setup for test of temperature and humidity probe

An Arduino C++ script converts the 41382VC outputted voltages (ranging from 0 V to 5 V for each parameter) into physical values—at 10-second intervals—according to the datasheet’s listed ranges [36]. The intermediate operation involves the Arduino Mega’s 10-bit analog-to-digital converter (ADC), implying mappings of nonnegative integers less than 1024 to each corresponding range. For this test, the measured and converted quantities manually transfer to a text file; a separate Python script then employs the Matplotlib library to yield graphical data.

Specifically, the final temporal resolution stands at one minute (60 seconds); for each parameter, every six values average into a singular quantity corresponding to one minute of time. Figure 31 displays the resultant temperature and humidity line graphs; the titular timestamp (in Peru Time) refers to the beginning of the test—i.e., minute zero.

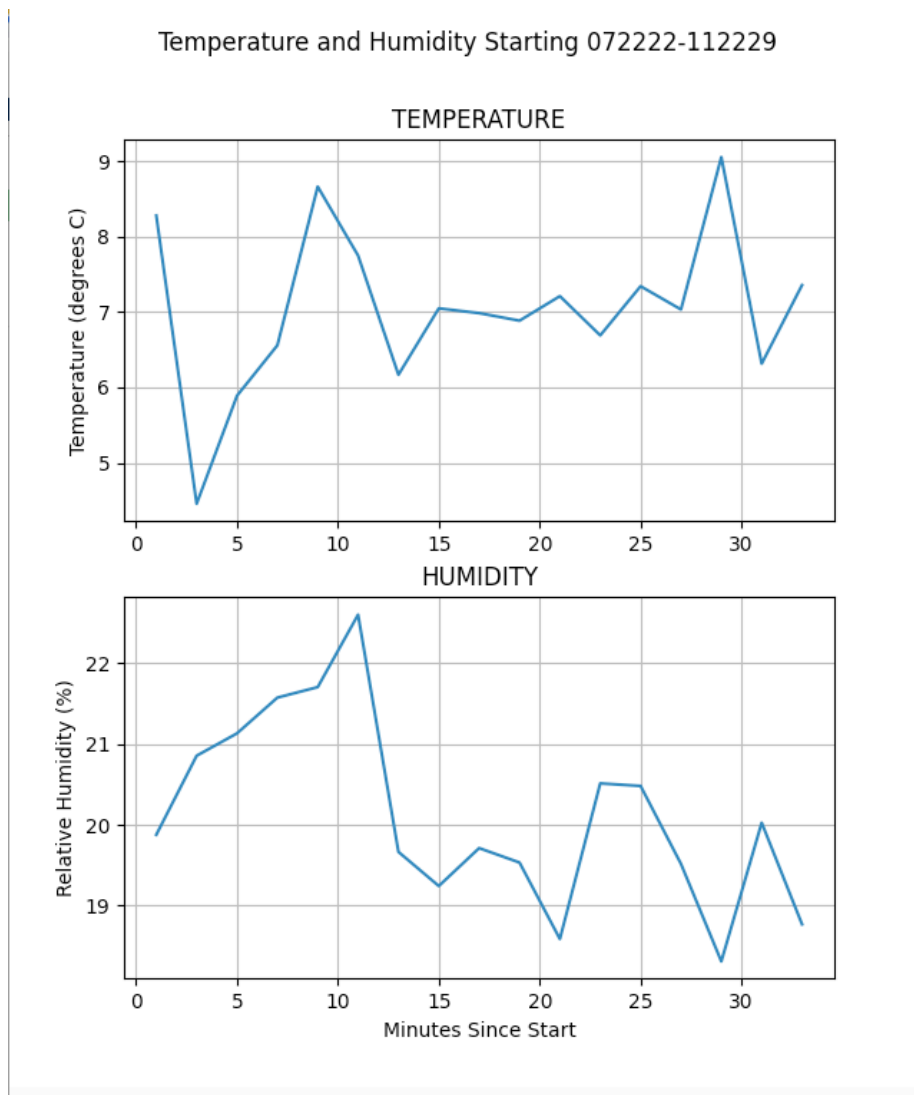


Figure 31: Temperature and humidity plots from the 41382VC probe test in Peru

Gas Analyzer: Due to the unavailability of the LI-850 instrument during the visit to Peru, all current testing of the device remains locationally confined to the Penn State University Park campus. Specifically, trials conducted on 18 October 2022 attempted to determine the efficacy of the data acquisition method: direct voltage outputs. A software interface—displaying real-time temporal plots of CO₂ and H₂O concentration values (in units of μmol/mol and mmol/mol, respectively)—comprises the main data logging subsystem; however, the previously discussed remote nature of deployments necessitates utilizing the LI-850's terminal block, consisting of a differential output pair for each variable.

Nevertheless, proper device operation warrants initial calibration of the variable ranges via the software. The user-set boundaries for CO₂ and H₂O, able to hold for extended missions after a single calibration, map to voltage ranges defined by a minimum of 0 V and a maximum of either 2.5 V or 5 V. Acquiring a voltage reading and subsequently converting it to its respective concentration value enables comparison between this 'indirectly obtained' quantity and the one directly displayed on the software interface. For this particular test (the hardware realization of which comprises Figure 32), a voltage range of 0 V to 5 V corresponds to each of the following ranges: 0 to 1000 μmol/mol CO₂ and 0 to 30 mmol/mol H₂O.



Figure 32: Testing implementation for the LI-850 Gas Analyzer

The measurements employed for preliminary evaluation characterize the ground-floor lobby of Atherton Hall (located in the southeastern part of Penn State’s campus) around 20:40 Eastern Daylight Time (EDT) on 18 October 2022. Because the acquired values define only two single instants in time at one indoor location, the closeness of the measured outputs to the ‘nominal’ software-displayed figures imply not necessarily general device effectiveness, but only the accuracy of the calibration at the respective time and location. Table 8 enumerates the results of the experiment.

Table 8: Results of preliminary gas analyzer test on 10/18/2022 at 20:40 EDT

VARIABLE	Carbon Dioxide (CO₂)	Water Vapor (H₂O)
<i>Software Reading</i>	637 $\mu\text{mol/mol}$	19.64 mmol/mol
<i>Measured Voltage</i>	3.175 V (0-5 V range)	3.180 V (0-5 V range)
<i>Deduced Measurement Value</i>	635 $\mu\text{mol/mol}$	19.08 mmol/mol
<i>Percent Difference</i>	0.31%	2.85%

Data Logger and Power Supply Testing

As implied in the preceding section, repeated failure of the SD card reader circuit and time constraints related to the gas analyzer precluded substantive testing of the data logging system. However, the very acquisition of direct voltage readings—thereby enabling conversion to temperature, humidity, and gas concentration values—speaks to the effectiveness of the logging mechanism, particularly for the warranted remote application. The primary auxiliary testing, therefore, concerns the performance of the sensors and Arduino when supplied power by the portable batteries—in addition to the solar panel’s charging thereof.

Directly observing such a battery charging setup—photographed below in Figure 33—on 22 July 2022 at HYO conveys the method’s efficacy. The north-facing solar panel efficiently harnesses the sunlight and (according to the panel’s indicator LEDs) restores a partially depleted LiFePO₄ battery (employed in the 41382VC probe tests) in approximately 20 minutes.



Figure 33: Testing setup for solar battery charger on 22 July at HYO

Likewise, the batteries themselves demonstrate the ability to sufficiently power the temperature and humidity probe, the gas analyzer, and the Arduino Mega module (via the DC-to-AC inverter). All such components exhibit signs of operation—including data outputting in the case of the sensors—when properly connected to the terminals of either battery. Combined with the demonstrated effectiveness of the solar battery charger, such a result implies reliability of the power subsystem, particularly for deployments in areas (like HYO and the surrounding region) receiving frequent high-intensity sunlight.

Chapter 5

Evaluating and Discussing the Test Results

The data collected by all integrated devices warrants an examination of the tests' collective efficacy—as well as that of the general engineering process. Most notably, the acquisition time frames fail to adequately encompass a reliable climate, or even air quality, study. The particle counter test—unexpectedly bolstered by a substantial fire event—indeed reveals changes due to the fire; in general, the PM mass concentrations (especially that of PM₁₀) increase while the probabilistic size distributions widen. However, the distribution shapes themselves remain rather similar, exhibiting heavy skews toward smaller particle sizes despite the noticeable post-fire change. Also, the eight distribution plots easily mislead viewers by virtue of their maximum size of 1.5 μm (compared to 10 μm in the Figure 29 reference plot). Fully acquiescing meaningful air quality information requires running additional spatial and temporal experiments (which entails testing in more environments and running several inter-day tests at each location).

Nevertheless, although the survey of particle size distribution around HYO remains unique to this study, the continuous operation of HYO's Grimm Portable Dust Monitor (pictured in Figure 19) enables comparative evaluation of the Handilaz Particle Counter's performance during the trials of 18 and 20 July 2022. Tables 9 and 10 enumerate the PM_{2.5} and PM₁₀ mass concentration values (in units of $\mu\text{g}/\text{m}^3$) obtained from the Handilaz counter readings and the simultaneous Grimm monitor recordings for the pre-fire (18 July) and post-fire (20 July) measurements, respectively [45]. Because the Grimm Portable Dust Monitor stands near the northwest corner of the HYO, the Handilaz Particle Counter measurements reported for this evaluation reflect those taken at Site 4 as labelled in Figure 28.

Table 9: Comparative PM2.5 and PM10 measurements for 18 July 2022

VARIABLE	Measurement Time (PET)	Grimm Portable Dust Monitor (stationary at HYO)	Handliaz Particle Counter (deployed at NW corner of HYO)
<i>PM2.5 ($\mu\text{g}/\text{m}^3$)</i>	16:11	3.3	2.3 (30.3% difference)
<i>PM10 ($\mu\text{g}/\text{m}^3$)</i>	16:11	6.4	16.9 (164% difference)

Table 10: Comparative PM2.5 and PM10 measurements for 20 July 2022

VARIABLE	Measurement Time (PET)	Grimm Portable Dust Monitor (stationary at HYO)	Handliaz Particle Counter (deployed at NW corner of HYO)
<i>PM2.5 ($\mu\text{g}/\text{m}^3$)</i>	12:15	0.7	3.1 (343% difference)
<i>PM10 ($\mu\text{g}/\text{m}^3$)</i>	12:15	1.8	61.0 (3289% difference)

Although the Handilaz readings indicate a substantial 261% increase in PM10 mass concentration following the 19 July mountainside fire, the stationary Grimm instrument yields unexpectedly low values for both variables at both time instants. This seems to indicate erratic, unreliable behavior by the portable Handilaz device; however, examining the complete July 2022 dataset for the Grimm monitor (collecting values at one-minute intervals) conveys otherwise. For example, in the minutes preceding the selected 20 July measurement, the Grimm monitor indicates a PM10 mass concentration of $2\mu\text{g}/\text{m}^3$ at 11:56 PET, a quantity which apparently jumps to

$10\mu\text{g}/\text{m}^3$ at 11:57 PET before regressing to an intermediate value, $5\mu\text{g}/\text{m}^3$, at 11:58 PET [45]. Of course, the known behavior of particulate matter highlights the physical impossibility of such a large concentration fluctuation in a mere two-minute period. Rather, such readings call into question the integrity of the Grimm sensory components or data logging system. With no other nearby PM instruments with which to compare the Handilaz readings, there remains a lack of reference for use in determining the relative accuracy of the particle counter. Only the ability to carry out measurements yielding real-time PM reports and particle size distributions, therefore, stems from the Handilaz device evaluation.

Likewise, not only does the temperature and humidity data (expressed graphically in Figure 31) exhibit a similar lack of substance; the instrument itself—coupled with its rudimentary Arduino C++ script—seemingly yields erroneous information. The average measured temperature of about 7°C differs significantly from other qualitative and quantitative observations conducted under the same spatial and temporal circumstances as the (detrimentally brief) 41382VC probe test. Moreover, the numbers themselves—converted from ADC values and incrementally averaged to generate the Figure 31 plots—source directly from the Arduino serial monitor as opposed to the more permanent and stable SD card. Prolonged analysis (the only experiment type to yield reliable ‘climate’ parameters) necessitates rectifying the aforementioned SD card reader issue and deploying the temperature and humidity sensor in several remote outdoor locations with the data logging program preloaded onto the Mega controller.

On the other hand, the relative accuracy exhibited by the LI-850 gas analyzer (as conveyed in Table 8) demonstrates its potential usefulness in a remote field study. Of course, the direct CO_2 and H_2O concentration readings stand with respect to those displayed via a USB connection to the same instrument; thus, the LI-850 measurements similarly lack proper references for stronger

performance assessment. Moreover, the previously discussed test—along with those exemplified by appendix graphics—only surveys a single location at two distinct time instants, thereby constituting almost no spatiotemporal resolution. Fully realizing the instrument’s ability to convey gas concentration trends over space and time (and to therefore bestow such knowledge upon Central Andean communities or other people) warrants additional extensive testing—including test deployments over periods exceeding several hours and in outdoor areas lacking immediate software interface access.

Similar assessments hold for the data logging and power subsystems. These primarily concern the generally unassessed robustness of the two LiFePO₄ batteries. Indeed, the only substantial battery power draw throughout the initial testing phase manifests itself as the 41382VC (temperature and humidity probe) and LI-850 (gas analyzer) trials; the Handilaz Particle Counter operates on its own lithium-ion battery. The short duration of the 41382VC test, moreover, warranted only a 20-minute-long recharge of the active battery with the solar panel. Such a sequence, while conveying the operational ability of power system, fails to quantify the full capacity of the batteries as it relates to deployment. That is, future tests with the two battery-dependent instruments operating simultaneously—and the batteries allowed to completely discharge within the safety margin—must necessarily precede actual system deployment. Such experiments will yield approximate ‘battery charge’ and ‘battery discharge’ times (specific to the sensors and data logger in question), from which one considers utilizing more LiFePO₄ batteries—or perhaps conservatively limiting each deployment to a single instrument.

Likewise, the powering of the Arduino Mega data logger through the DC-to-AC inverter stands as experimentally verified but severely limited in scope. Conducting additional tests with these components in conjunction with the sensory instruments offers to address this shortcoming.

Chapter 6

What's Next?

The incomplete nature of the component testing compels future experiments to determine the system's full potential for Central Andean deployment. With the three subsystems and the peripheral software (viz., the Arduino C++ data logging procedure and the particle counter Python script utilizing the Matplotlib library) in place, simply extending the spatial and temporal scope of testing comprises the next stage. The following section embodies such an extension, proposing a potential experiment to conduct with the current system in the Junín, Peru, communities of interest, Sicaya and Huayao.

Detailing Potential Future Experiments

Fully Testing the Power Supply: Carrying out a complete field profile with the system firstly requires assurance of a reliable power supply. As previously implied, this entails not only gauging the battery's per-capacity lifetime but also measuring the entire charge period provided by the solar battery charger. The previously conducted assessment harnesses sunlight in nearly full-intensity conditions—near solar noon with almost no cloud coverage. With the charging mechanism exclusively dependent on sunlight, continuously operating the panel under a variety of overcast conditions comprises an important step. Such considerations yield the following testing regimen (to be conducted at a Central Andes location, perhaps HYO) by which to assess the system power supply:

- Conduct three stationary tests with the 41382VC Temperature and Relative Humidity Probe, powering the instrument with one fully charged LiFePO₄ battery

and recording the operation time intervals (i.e., the time elapsed until the battery discharges).

- Conduct three identical stationary tests with the LI-850 Gas Analyzer.
- Operate the solar battery charger with a fully depleted LiFePO₄ battery on each day of a 14-day period, ensuring that the experiment samples several cloudiness conditions; actively monitor the solar panel so as to progressively orient it toward the Sun. For each day, record the meteorological conditions time elapsed for a full battery charge.

Verifying Instrument Performance: As mentioned, even the one instrument characterized by applicable data, the particle counter, lacks an adequate reference for quantitative evaluation. Therefore, further testing must necessarily entail comparison of acquired measurements to those yielded by reliable fixed instruments. The HYO weather station, photographed in Figure 18, offers to serve as a potential reference for the 41382VC temperature and relative humidity probe; additional devices comprising the broader Peruvian or global network of climate instruments may possibly accomplish the same end for the LI-850 Gas Analyzer.

Determining the System's Ease of Use: Of course, operation of the sensor network relies not only on component performance but also on the feasibility of direct community deployment. Compounded with the requirement for both spatial and temporal measurements, this fact warrants a series of tests involving volunteer residents of Sicaya and Huayao. Residential students—who comprised a significant portion of Sicaya's engagement session discussed in Chapter 1—stand ready to learn more about climate science and would, therefore, fit well into a study involving atmospheric instrumentation.

Pending IRB approval, a group consisting of perhaps six Huayao students and six Sicaya students could carry out several measurements. Working under supervision from an engineer familiar with the system, one student carrying the main instrumentation (enclosed in the larger Gratury junction box) and another carrying the spare battery (enclosed in the smaller box) and solar charger manifests itself as a possible experimental setup. While the nature of the power supply and the voltage outputs enables continuous operation of the 41382VC probe and the LI-850 analyzer, the mechanisms characterizing the Handilaz counter render continuous PM measurements impossible. Therefore, efficiency in such experiments derives from first selecting points of interest throughout the communities at which to assess PM; each walking path between a pair of such points defines the area for measuring temperature, relative humidity, and greenhouse gas concentrations. Thus, the mere portability of the sensors and auxiliary components bestows the spatial resolution seemingly precluded by the single-point operation of the particle counter. Figure 34 depicts potential points of interest in both Sicaya and Huayao; the need to assess both agricultural and personal facets affords a varied distribution of points among fields and population centers.



Figure 34: Potential measurement points for Huayao (top) and Sicaya (bottom) [11]

Graduating from outdoor sites to individual households—to measure not only PM concentrations but also the other four parameters, which remain conducive to both health and comfort—requires first gauging community interest in, and familiarity with, the system itself. The

experiment described here (involving volunteer students receiving operational training and traversing their respective towns) aims to achieve this.

Reflecting and Concluding

Of course, the scope and urgency of the climate change problem comparatively dwarf this project and its future objectives. Developing a single system—comprising only three instruments selected on the basis of two small communities in a single region of a single country—appears almost negligible in the face of the large-scale mitigation strategies climatologists deem necessary. Moreover, even the preliminary objective of understanding and quantifying the phenomenon seems out of reach with just five variables to assess, and only the mere *potential* feasibility of the system components emerges from the project's current stage.

However, one critical aspect of this particular design process stands out as lacking in most other climate research endeavors: community engagement. Rather than blanketly employing global climate change as a motivation for better understanding it, this project explores the lives and practices of groups that best exemplify climate change vulnerability: agricultural communities in a rural region of a developing country. When one sets aside broad studies or international governmental reports and actually observes both lives and lifestyles at stake, he or she becomes instilled with an even stronger motivation to save such lives and to preserve such lifestyles. Including a temperature and humidity probe stems not only from these variables' relevance to weather and climate but, more importantly, from residents' curiosities regarding extreme temperature phenomena. Packaging a handheld particle counter results from testified and observed respiratory health issues among the people—not solely from the desire to measure air quality.

Similar tenets justify the inclusion of a CO₂ and H₂O analyzer. Likewise, designing the system as easily teachable and accessible eliminates the researcher-stakeholder ‘knowledge gap’ that often characterizes academic studies; allowing community members direct system access facilitates their acquisition of knowledge and empowers them to ask their own scientific questions that outside researchers often overlook.

Of course, this project falls far short of solving global climate change—and even of identifying and pinpointing its causes. Countless other variables of interest, most notably nitrogen dioxide and ozone, remain crucially relevant yet fail to comprise the portable system parameters. However, these broad objectives never characterized the goal of this individual project. If this research accomplishes anything, it is to inspire others to adopt similar community-based approaches to combatting humanity’s greatest challenge. Living among and engaging with people from all regions enables one to design measurement systems, or even direct solutions, based on experience and first-hand account. Not only does each individual project like this stand to educate and assist people in need; a collection of such projects, each one uniquely and intimately tailored to a specific community, promotes global knowledge and catalyzes global mitigation efforts, leading to an eventual reversal of the phenomenon—and an overall betterment of humanity.

BIBLIOGRAPHY

- [1] “Solutions,” *Project Drawdown*, 13-Jun-2022. [Online]. Available: <https://drawdown.org/solutions>. [Accessed: 20-Jun-2022].
- [2] O. A. Galagarza, A. Ramirez-Hernandez, H. F. Oliver, and A. J. Deering, *Map of Peru, showing its three geographical regions and 25 departments*. 2021. ArcGIS 10.8.1 software (<http://www.esri.com/software/arcgis>, accessed on 5 May 2021) was used to develop the map.
- [3] Aladin, “Lima, Peru - climate & monthly weather forecast,” *Weather Atlas*. [Online]. Available: <https://www.weather-atlas.com/en/peru/lima-climate>. [Accessed: 04-Oct-2022].
- [4] “El Niño and Its Effects,” *El Niño and Southern Oscillation*. [Online]. Available: http://earthguide.ucsd.edu/virtualmuseum/climatechange1/11_1.shtml. [Accessed: 04-Oct-2022].
- [5] B. J. Ranson, “The Ultimate Resource for World Climate and biomes,” *Geodiode*, 2022. [Online]. Available: <https://geodiode.com/climate/lima>. [Accessed: 04-Oct-2022].
- [6] J. Oviden, “Extreme Weather Events in Peru,” 25-Jun-2022.
- [7] C. Rodríguez-Morata, H. F. Díaz, J. A. Ballesteros-Canovas, M. Rohrer, and M. Stoffel, “The anomalous 2017 coastal El Niño event in Peru,” *Climate Dynamics*, vol. 52, no. 9-10, pp. 5605–5622, Sep. 2018.
- [8] “World Bank Climate Change Knowledge Portal,” *Climatology | Climate Change Knowledge Portal*, 2021. [Online]. Available: <https://climateknowledgeportal.worldbank.org/country/peru/climate-data-historical>. [Accessed: 04-Oct-2022].
- [9] K. Leperi, *Grand Amazon Lodge*. 2022. [Online]. Available: <https://www.hotel-scoop.com/wp-content/uploads/2020/06/7R401459.jpg>. [Accessed: 04-Oct-2022].
- [10] *Cusco monthly climate data: temperature and precipitation*. [Online]. Available: <https://www.climatestotravel.com/images/charts/Cusco-Peru.png>. [Accessed: 05-Oct-2022].
- [11] *Google maps*. [Online]. Available: <https://www.google.com/maps>. [Accessed: 18-Jul-2022].

- [12] R. Zubieta, F. Prudencio, Y. Ccanchi, M. Saavedra, J. Sulca, J. Reupo, and G. Alarco, “Potential conditions for fire occurrence in vegetation in the Peruvian Andes,” *International Journal of Wildland Fire*, vol. 30, no. 11, pp. 836–849, Oct. 2021.
- [13] C. E. Forest, “A Brief Overview of Climate Change and Impacts,” in *2022 Peru iRES, Penn State University*, 15-Jul-2022.
- [14] C. E. Forest and A. J. DeMarchis, “Huayao Community Engagement - 2022 Peru iRES, Penn State University.” Huayao, Junín, Peru, 09-Jul-2022.
- [15] V. P. Llactayo and A. J. DeMarchis, “Sicaya Community Engagement - 2022 Peru iRES, Penn State University.” Sicaya, Junín, Peru, 15-Jul-2022.
- [16] B. G. Fejer, D. L. Hysell, and L. A. Navarro, “Anomalous electron temperature increases in the evening equatorial ionosphere,” *Journal of Geophysical Research: Space Physics*, vol. 126, no. 2, Jan. 2021.
- [17] N. M. Pedatella, J. L. Chau, J. Vierinen, L. Qian, P. Reyes, E. Kudeki, G. Lehmacher, and M. Oppenheim, “Solar flare effects on 150-km echoes observed over jicamarca: WACCM-X simulations,” *Geophysical Research Letters*, vol. 46, no. 20, pp. 10951–10958, Oct. 2019.
- [18] A. Gettelman, M. J. Mills, D. E. Kinnison, R. R. Garcia, A. K. Smith, D. R. Marsh, S. Tilmes, F. Vitt, C. G. Bardeen, J. McInerney, H. L. Liu, S. C. Solomon, L. M. Polvani, L. K. Emmons, J. F. Lamarque, J. H. Richter, A. S. Glanville, J. T. Bacmeister, A. S. Phillips, R. B. Neale, I. R. Simpson, A. K. DuVivier, A. Hodzic, and W. J. Randel, “The whole atmosphere community climate model version 6 (WACCM6),” *Journal of Geophysical Research: Atmospheres*, vol. 124, no. 23, pp. 12380–12403, Dec. 2019.
- [19] I. Cnossen, “Analysis and attribution of climate change in the upper atmosphere from 1950 to 2015 simulated by waccm-x,” *Journal of Geophysical Research: Space Physics*, vol. 125, no. 12, Nov. 2020.
- [20] J. L. Flores-Rojas, Y. Silva, L. Suárez-Salas, R. Estevan, J. Valdivia-Prado, M. Saavedra, L. Giraldez, M. Piñas-Laura, D. Scipión, M. Milla, S. Kumar, and D. Martinez-Castro, “Analysis of extreme meteorological events in the Central Andes of Peru using a set of specialized instruments,” *Atmosphere*, vol. 12, no. 3, p. 408, Mar. 2021.
- [21] J. L. Flores-Rojas, “Temperature and humidity data from Huancayo Observatory Gradient Tower for month of July 2022.” Huancayo Observatory, Huancayo, Junín, Peru, 01-Aug-2022.
- [22] J. L. Gupta, *Acute Respiratory Infections in Central Andean Populations due to Aerosols*, Huancayo, Junín, Peru - Penn State University, 2022.

- [23] W. M. Barea, *Black carbon and how it affects the Huaytapallana glacier in the Central Andes of Peru*, Huancayo, Junín, Peru – Penn State University, 2022.
- [24] *Tropospheric ozone global averages*. Climate & Clean Air Coalition. http://ccacoalition.org/sites/default/files/uploaded/ozone-emissions-background_0.png
- [25] *Tropospheric ozone production*. LADCO. https://www.ladco.org/wp-content/uploads/2018/09/O3_Schematic-467x350.png
- [26] J. M. Valdivia, D. A. Guizado, J. L. Flores-Rojas, D. P. Gamarra, Y. F. Silva-Vidal, and E. R. Huamán, “Field campaign evaluation of Sensors Lufft GMX500 and Maximet WS100 in Peruvian Central Andes,” *Sensors*, vol. 22, no. 9, p. 3219, 2022.
- [27] N. Wildmann, R. Eckert, A. Dörnbrack, S. Gisinger, M. Rapp, K. Ohlmann, and A. van Niekerk, “In situ measurements of wind and turbulence by a motor glider in the Andes,” *Journal of Atmospheric and Oceanic Technology*, vol. 38, no. 4, pp. 921–935, Apr. 2021.
- [28] S.-A. Arghirescu, M. Drăgan, and O. Fratu, “Footprint reduction of sensor control modules for Remote Portable Laboratories,” *Sensors*, vol. 22, no. 4, p. 1483, Feb. 2022.
- [29] L. Nicolaou, M. Fandiño-Del-Rio, K. Koehler, and W. Checkley, “Size distribution and lung-deposited doses of particulate matter from household exposure to biomass smoke,” *Wiley*, pp. 51–62, Jun. 2020.
- [30] J. L. Kephart, M. Fandiño-Del-Rio, K. N. Williams, G. Malpartida, K. Steenland, L. P. Naeher, G. F. Gonzales, M. Chiang, W. Checkley, K. Koehler, J. Rosenthal, T. Aguilar, V. Burrowes, E. C. Fung, D. Goodman, S. A. Harvey, P. Herrera, A. Lee, K. A. Lee, C. H. Miele, M. Moazzami, L. H. Moulton, S. Nangia, C. O’Brien, S. Simkovich, T. Shade, L. Stashko, and A. Villegas-Gomez, “Nitrogen Dioxide exposures from biomass cookstoves in the Peruvian Andes,” *Indoor Air*, vol. 30, no. 4, pp. 735–744, Feb. 2020.
- [31] Y. Romero, R. M. Velásquez, and J. Noel, “Development of a multiple regression model to calibrate a low-cost sensor considering reference measurements and meteorological parameters,” *Environmental Monitoring and Assessment*, vol. 192, no. 8, p. 498, Jul. 2020.
- [32] Y.-S. Hwang, J.-J. Lee, S.-I. Park, and J.-S. Um, “Exploring explainable range of in-situ portable CO₂ sensor signatures for Carbon Stock estimated in Forestry Carbon Project,” *Sensors and Materials*, vol. 31, no. 11, p. 3773, 2019.
- [33] T. Shah, *Can Solar Cookers Address Fossil Fuel Dependency?*, Huancayo, Junín, Peru - Penn State University, 2022.
- [34] *Climate Change: Atmospheric Carbon Dioxide*. NOAA Climate.gov. https://www.climate.gov/sites/default/files/styles/full_width_620_original_image/public/

- 2021-10/ClimateDashboard-atmospheric-carbon-dioxide-graph-20211004-1400px.jpg?itok=W57BtpJB
- [35] *RM Young 41382VC, Relative Humidity/Temperature Probe*. Amazon.com. https://m.media-amazon.com/images/I/21oOJYNLLsS._SX342_.jpg
- [36] *Relative Humidity/Temperature Probe with Voltage Output*. 41382VC. Rev. F111215. RM Young Company.
- [37] *Handheld Particle Counter: Handilaz Mini II*. Particle Measuring Systems. <https://www.pmeasuring.com/wp-content/uploads/2019/10/HandiLaz-Mini-2019.png>
- [38] *HandiLaz Mini II Handheld Airborne Particle Counter*. Particle Measuring Systems.
- [39] *LI-830 and LI-850*. LI-COR Biosciences. <https://www.licor.com/env/support/LI-850/images/830-850.png>
- [40] *Using the LI-850 and LI-830 Gas Analyzers*. LI-850. Rev. 17190. LI-COR Biosciences.
- [41] *Nermak 12V 12Ah LiFePO4 Deep Cycle Battery*. Amazon. https://m.media-amazon.com/images/I/61m+XxSBtyL._AC_SL1500_.jpg
- [42] *BESTEK 300W Power Inverter DC 12V to 110V AC Car Inverter with 4.2A Dual USB Car Adapter*. Amazon. <https://m.media-amazon.com/images/I/7164SYS5GUL.jpg>
- [43] *SUNER POWER Waterproof 12V Solar Battery Charger & Maintainer Pro*. Amazon. https://m.media-amazon.com/images/I/81urjWy+1-L._AC_SL1500_.jpg
- [44] *Compass Icon Wind Map North West Vector Stock Illustration*. Dreamstime. <https://thumbs.dreamstime.com/b/compass-icon-wind-map-north-west-vector-illustration-179814566.jpg>
- [45] L. F. Suarez Salas, “Particulate matter concentration data from Huancayo Observatory Grimm Portable Dust Monitor for month of July 2022.” Huancayo Observatory, Huancayo, Junín, Peru, 22-Jul-2022.

ACADEMIC VITA – Antonio DeMarchis

Skills

-
- Python: Developed testing & data automation tools
 - LabVIEW: Secured Associate Developer Certificate
 - MATLAB: Analyzed and designed electrical devices
 - SolidWorks: Modeled toy locomotive & sock aid
 - Tutoring: Volunteered two hours per week with HKN
 - Robotics: Built cleaning robot through TI sponsorship
 - Sensors: Designed controller-based air quality monitor
 - Technical Writing: Authored undergraduate thesis

Education

-
- **Penn State University Schreyer Honors College: B.S., Electrical Engineering** August 2019 – December 2022
 - Relevant Coursework: Linear Electronic Circuits; Energy Conversion; Capstone Design Project; Power Electronics; Technical Writing; Design Process; Electromagnetics; Nanoelectronics; Design Tools; Probability for Electrical Engineers; Electronic Circuit Design I & II; Continuous-Time Linear Systems; Honors Discrete Math

Work Experience

-
- **Electrical Engineering Intern, Burns Engineering, Inc.** May 2021 – December 2021
 - Automated Amtrak field test procedures and transponder data analysis
 - Enabled 160mph testing capabilities on Amtrak's ACSES/ATC simulator
 - **Electrical Engineering Intern, Westinghouse Electric Company** May 2020 – August 2020
 - Designed Feedwater Level Control System upgrade for River Bend Station
 - Co-authored three power calculations and verified over 100 wire terminations
 - **Mathematics Instructor, Mathnasium of Murrysville** July 2018 – August 2019
 - Tutored over 50 K-12 students to improve their grades and evoke their love for mathematics
 - Consulted families regarding student progress; customized study plan for each student's success

Leadership Roles

-
- **Teaching Assistant, Spring 2022 Freshman Seminar** January 2022 – May 2022
 - Prepared course materials related to microcontrollers and remote sensing
 - Guided students through lab exercises; facilitated conceptual discussions
 - **Eta Kappa Nu (HKN) Epsilon Chapter**
 - President April 2021 – April 2022
 - Presided over all club operations (meetings, tutoring, event planning, etc.)
 - Led seven-member officer board; planned tutoring and EECS outreach sessions
 - Tutoring Coordinator December 2020 – April 2021
 - Oversaw 13 weekly peer tutoring sessions in EECS courses; assisted up to five students per week
 - **Institute for Electrical and Electronics Engineers (IEEE) Student Chapter**
 - Corporate Relations Liaison April 2021 – April 2022
 - Managed over 15 company partnerships; guiding Communications Chair
 - Coordinated Lockheed Martin electronic cornhole student design competition
 - Communications Chair September 2020 – April 2021
 - Planned over 10 corporate events to bolster companies' recruitment efforts
 - Acquired club sponsorships through company outreach and collaboration
 - **International Undergraduate Research** September 2021 – November 2022
 - Designed mobile weather station; researched component specifications and prepared thesis
 - Built sensor network alongside Peru students to test in various terrains